

GAS TURBINE REHEAT USING IN-SITU COMBUSTION

**Topical Report:
Task 1 – Blade Path Aerodynamics**

by

**T.E. Lippert
D.M. Bachovchin**

April 30, 2004

Cooperative Agreement No. DE-FC26-00NT40913

**Siemens Westinghouse Power Corporation
4400 Alafaya Trail
Orlando, FL 32826**

**and
P.G.A. Cizmas
Texas A&M University
College Station, TX 77843-3141**

Prepared for

**U.S. Department of Energy
National Energy Technology Laboratory
3610 Collins Ferry Road
P. O. Box 880
Morgantown, WV 26507-0880**

Charles Alsup — DOE/NETL Project Manager

DISCLAIMER

This report was prepared as an account of work sponsored by the United States Government. Neither the United States nor the United States Department of Energy, nor any of their employees, makes any warranty, expressed or implied, or assumes any legal liability or responsibility for the accuracy, completeness, or usefulness of any information, apparatus, product, or process disclosed, or represents that its use would not infringe privately owned rights. Reference herein to any specific commercial product, process, or service by trade name, mark, manufacturer, or otherwise, does not necessarily constitute or imply its endorsement, recommendation, or favoring by the United States Government or any agency thereof. The views and opinions of authors expressed herein do not necessarily state or reflect those of the United States Government or any agency thereof.

ABSTRACT

Siemens Westinghouse Power Corporation (SWPC) is developing in-situ reheat (fuel injection via airfoil injection) as a means for increasing cycle efficiency and power output, with possibly reduced emissions. In addition to kinetic modeling and experimental work, CFD modeling (by Texas A&M) of airfoil injection and its effects on blade aerodynamics and turbine performance. This report discusses validation of the model against single-vane combustion test data from Siemens Westinghouse, and parametric studies of injection reheat in a modern turbine. The best location for injection is at the trailing edge of the inlet guide vane. Combustion is incomplete at trailing edges of subsequent vanes. Recommendations for further development are presented.

FOREWORD

Cooperative Agreement No. DE-FC26-00NT40913, "Gas Turbine Reheat Using In-Situ Combustion," between Siemens Westinghouse Power Corporation and the United States Department of Energy began on October 1, 2000, and is scheduled to end on May 31, 2004.

The overall objective of this project is to develop a novel gas reheat concept for gas turbine engines, in which fuel is injected directly into the turbine through one or more stages of vanes and/or blades. The key research goals involved in concept selection are to understand the combustion kinetics (burnout, emissions), blade performance and effects on turbine power output and efficiency. The concept is being evaluated for maximum energy efficiency (full reheat) and as a means to achieve power boost (minimum reheat)

Background. Increasing gas turbine firing temperature has historically increased gas turbine efficiency and power output. This approach is limited by the generation of thermal NO_x and by the need for advanced materials at higher temperatures.

A well-known alternative approach is to add reheat combustion between turbine stages to achieve higher mean temperatures at which heat is extracted, without increasing maximum temperature. More fuel is burned, to give higher power output. If this is accompanied by increased pressure ratio, or used in combined cycle with higher steam cycle inlet temperature, then cycle efficiency is also increased.

Prior suggested reheat schemes have used discrete reheat combustors, either within a larger shell or externally, between two separate turbines. In the concept of this work, reheat fuel is injected directly into the turbine flow via injection holes in the turbine vanes or blades. The advantages are: 1) simplicity in turbine design with no increase in casing size and no external reheat combustor and transition. 2) Lower reheat peak combustion temperature; 3) near zero reheat NO_x formation, with normalized NO_x (to 15% oxygen) actually reduced; 4) reduced parasitic pressure loss; 5) substitution of fuel for some airfoil coolant flow.

Relevancy. The in-situ reheat concept represents a new approach that can allow gas turbine engines to move toward DOE goals of higher efficiency, higher power output, low emissions engines. This work will develop the scientific basis for the concept of in-situ reheat. In particular the work will identify the combustion kinetic basis for injection, will identify practical designs (simple or flame-held) for achieving injection, and will quantify effects on airfoil aerodynamics and turbine performance.

The project is divided into four technical tasks:

Task 1, Blade Path Aerodynamics (performed by Texas A&M University). A CFD model, CoRSI (Combustion and Rotor-Stator Interaction) was to incorporate simplified combustion kinetics with blade path flow. The model was used to investigate the effect of injection parameters (stage, fuel flow, fuel temperature, injection angle) on turbine performance (burnout location, forces on blades, power output, efficiency).

Task 2, Combustion and Emissions. Detailed (Chemkin and GRI data base) calculations are being performed to characterize reheat fuel burnout and emissions kinetics. Calculations are aimed at flameless (simple injection) and flame-held injection designs.

Task 3, Sub-Scale Testing. Direct injection is being studied experimentally in high-pressure, high-temperature test rigs. Blade path temperatures and velocities are used, with reduced pressure. The progress of direct injection combustion is being measured as a function of residence time. Results are used to calibrate Task 2 modeling and to check Task 1 model results.

Task 4, Conceptual Design and Development Plan. A preferred design approach will be identified and prepared for pre-commercial development based on the results of prior tasks.

The present document is the required Topical Report on Task 1.

Blade Path Aerodynamics for Gas Turbine In-Situ Reheat Combustion

Paul G. A. Cizmas
Department of Aerospace Engineering
Texas A&M University
College Station, TX 77843-3141

Prepared for Siemens Westinghouse Power Corporation

March 31, 2004

LIST OF FIGURES	viii
LIST OF TABLES	IX
NOMENCLATURE	X
EXECUTIVE SUMMARY	1
1. INTRODUCTION AND BACKGROUND	3
2. GENERAL MODELING PROCEDURE	4
PHYSICAL MODEL	4
<i>Governing Equations</i>	4
<i>Chemistry Model</i>	5
NUMERICAL MODEL	5
<i>Grid Generation</i>	5
<i>Discretization of Governing Equations</i>	6
<i>Boundary Conditions</i>	6
3. EXPERIMENTAL POINTS	8
APPROACH	8
<i>Case 3B1</i>	9
<i>Case 4B2</i>	10
TWO-DIMENSIONAL MODEL	10
<i>Case 3B1</i>	10
Large injector length	11
Small injector length	12
Medium injector length	13
<i>Case 4B2</i>	16
Large injector length	17
Small injector length	18
THREE-DIMENSIONAL MODEL	19
4. INDUSTRIAL GAS TURBINE SIMULATIONS	26
APPROACH	27
<i>Geometry and Flow Conditions</i>	27
<i>Accuracy of Numerical Results</i>	27
RUN SET 1	28
RUN SET 2	35
<i>Four-stage turbine</i>	38
<i>Five-stage turbine</i>	41
<i>Run Set 3</i>	44
5. CONCLUSIONS	49
6. RECOMMENDATIONS	50
REFERENCES	51

List of Figures

FIGURE 1. EXPERIMENTAL APPARATUS.	8
FIGURE 2. COMBUSTION PROBE.	9
FIGURE 3. TOTAL TEMPERATURE CONTOURS FOR CASE 3B1. TOP: LARGE WIDTH, MIDDLE: MEDIUM WIDTH, BOTTOM: SMALL WIDTH INJECTOR	14
FIGURE 4. MOLE FRACTION CONTOURS FOR CASE 3B1. TOP: LARGE WIDTH, MIDDLE: MEDIUM WIDTH, BOTTOM: SMALL WIDTH INJECTOR.....	15
FIGURE 5. METHANE MOLE FRACTION AT SEVERAL LOCATIONS ALONG THE SAMPLE SECTION. TOP: LARGE WIDTH, MIDDLE: MEDIUM WIDTH, BOTTOM: SMALL WIDTH INJECTOR.....	16
FIGURE 6. DETAIL OF THE COMPUTATIONAL DOMAIN OF THE SINGLE-VANE BURNER.....	19
FIGURE 7. DETAIL OF THE SINGLE-VANE BURNER GRID.	20
FIGURE 8. CONTOUR PLOTS OF METHANE.	22
FIGURE 9. CONTOUR PLOTS OF METHANE IN x =CONSTANT PLANES.	22
FIGURE 10. METHANE MOLE FRACTION Z-PLANE CONTOUR PLOTS. THE $z = 0.0$ IS THE SAME AS SHOWN IN FIGURE 8.	23
FIGURE 11. CONTOUR PLOTS OF CO	23
FIGURE 12. CONTOUR PLOTS OF CO AT x =CONSTANT PLANES.....	24
FIGURE 13. CARBON MONOXIDE MOLE FRACTION Z-PLANE CONTOUR PLOTS. THE $z = 0.0$ IS THE SAME AS SHOWN IN FIGURE 11.....	24
FIGURE 14. CONTOUR PLOTS OF TOTAL TEMPERATURE.	25
FIGURE 15. CONTOUR PLOTS OF TOTAL TEMPERATURE AT x =CONSTANT PLANES.....	25
FIGURE 16. TOTAL TEMPERATURE Z-PLANE CONTOUR PLOTS. THE $z = 0.0$ IS THE SAME AS SHOWN IN FIGURE 14.	26
FIGURE 17. DETAIL OF THE MEDIUM GRID (EVERY OTHER GRID POINT IN EACH DIRECTION SHOWN).....	28
FIGURE 18. STATIC PRESSURE ON FIRST ROW OF VANES IN THE CASE WITHOUT COMBUSTION.	29
FIGURE 19. VARIATION OF AVERAGED TOTAL ENTHALPY (ABSOLUTE OR RELATIVE).	31
FIGURE 20. VARIATION OF STAGNATION TEMPERATURE ALONG FIRST ROW OF ROTORS FOR THE CASE WITHOUT COMBUSTION AND CASE C1YHF OF <i>IN SITU</i> REHEAT.	31
FIGURE 21. VARIATION OF CH_4, O_2, CO_2 AND H_2O MASS FRACTIONS ALONG THE TURBINE.	35
FIGURE 22. OXYGEN CONTOURS AND VELOCITY VECTORS NEAR THE INJECTION LOCATION FOR CASES 2 AND 2WIDE.	38
FIGURE 23. OXYGEN CONTOURS FOR CASES 1 THROUGH 5.	39
FIGURE 24. OXYGEN CONTOURS AND VELOCITY VECTORS NEAR THE INJECTION LOCATION FOR CASE 4.	40
FIGURE 25. TEMPERATURE CONTOURS FOR CASES 1 THROUGH 5.....	41
FIGURE 26. OXYGEN CONTOURS FOR CASES 7 THROUGH 10.	42
FIGURE 27. TEMPERATURE CONTOURS FOR CASES 6 THROUGH 10.	43
FIGURE 28. OXYGEN CONTOURS AND VELOCITY VECTORS FOR CASES 3 AND 8.	44
FIGURE 29. OXYGEN CONTOURS FOR CASES C THROUGH K.	47
FIGURE 30. TEMPERATURE CONTOURS FOR CASES B THROUGH K.	48

List of Tables

TABLE 1. GAS MIXTURE MOLAR COMPOSITION %, CASE 3B1	9
TABLE 2. INJECTION FUEL MOLAR COMPOSITION %, CASE 3B1	10
TABLE 3. GAS MIXTURE MOLAR COMPOSITION %, CASE 4B2	10
TABLE 4. INJECTION FUEL MOLAR COMPOSITION %, CASE 4B2	10
TABLE 5. SPECIES MOLE FRACTION % AT 0.311 M DOWNSTREAM FOR CASE 3B1 WHILE USING LARGE SIZE INJECTOR	11
TABLE 6. SPECIES MOLE FRACTION % AT 0.654 M DOWNSTREAM FOR CASE 3B1 WHILE USING LARGE SIZE INJECTOR	11
TABLE 7. TEMPERATURE VALUES FOR LARGE SIZE INJECTOR, CASE 3B1. EXPERIMENTAL VALUE AT 0.836 M IS 1478 K.	12
TABLE 8. SPECIES MOLE FRACTION % AT 0.311 M DOWNSTREAM FOR CASE 3B1 USING SMALL SIZE INJECTOR	12
TABLE 9. SPECIES MOLE FRACTION % AT 0.654 M DOWNSTREAM FOR CASE 3B1 USING SMALL SIZE INJECTOR	12
TABLE 10. TEMPERATURE VALUES FOR SMALL SIZE INJECTOR, CASE 3B1. EXPERIMENTAL VALUE AT 0.836 M IS 1478 K.	13
TABLE 11. SPECIES MOLE FRACTION % AT 0.311 M DOWNSTREAM FOR CASE 3B1 USING THE MEDIUM SIZE INJECTION.	13
TABLE 12. SPECIES MOLE FRACTION % AT 0.654 M DOWNSTREAM FOR CASE 3B1 USING THE MEDIUM SIZE INJECTION.	13
TABLE 13. TEMPERATURE VALUES FOR MEDIUM SIZE INJECTOR, CASE 3B1. EXPERIMENTAL VALUE AT 0.836 M IS 1478 K.	13
TABLE 14. SPECIES MOLE FRACTION % AT 0.765 M DOWNSTREAM FOR CASE 4B2	17
TABLE 15. SPECIES MOLE FRACTION % AT 1.059 M DOWNSTREAM FOR CASE 4B2	17
TABLE 16. TEMPERATURE VALUES AT REQUESTED LOCATIONS FOR CASE 4B2. EXPERIMENTAL VALUE AT 0.84 M IS 1252 K.	17
TABLE 17. SPECIES MOLE FRACTION % AT 0.765 M DOWNSTREAM FOR CASE 4B2	18
TABLE 18. SPECIES MOLE FRACTION % AT 1.059 M DOWNSTREAM FOR CASE 4B2	18
TABLE 19. TEMPERATURE VALUES AT REQUESTED LOCATIONS FOR CASE 4B2. EXPERIMENTAL VALUE AT 0.84 M IS 1252 K.	18
TABLE 20. INPUT DATA FOR THE VANE-BURNER	21

Nomenclature

$p_{-\infty}$	turbine inlet static pressure (bar)
$T_{-\infty}$	turbine inlet static temperature (K)
$Re_{-\infty}$	turbine inlet Reynolds number based on the first vane axial chord
$p_{exit} / p_{-\infty}^*$	ratio between turbine exit static temperature and turbine inlet stagnation temperature
p_{hole}	static pressure at the injection hole (bar)
T_{hole}	static temperature at the injection hole (K)
V_{hole}	velocity of the injected fuel (m/s)
h	static enthalpy
h_w^*	stagnation enthalpy based on the relative velocity (for rotors)
T_w^*	stagnation temperature based on the relative velocity (for rotors)
h^*	stagnation enthalpy based on the relative velocity (for stators)
T^*	stagnation temperature based on the relative velocity (for stators)
ΔP	overall power increase of the turbine relative to the case without injection
X_i	mass fraction of species i
\dot{W}_{CH_4}	mass flow of injected methane (kg/s/mm vane span/vane)
S	the mixedness parameter (see definition on page 33)
S_{bl}	interblade pitch

Executive Summary

Current conventional developments of gas turbine aero thermodynamics provide small efficiency and power increase, because with the present technology one reached an asymptotical convergence to the upper limit of the gas turbine performance. This asymptotical convergence implies that large efforts to ameliorate the aerothermodynamics result in rather small improvements. Turbine combustion provides a paradigm shift and a step change in gas turbine aerothermodynamics.

This report presents the experimental and computational investigation of *in situ* reheat in turbine-combustors. A turbine-combustor is defined as a turbine in which fuel is injected and combusted. The process of combustion in the turbine is called *in situ* reheat. Thermodynamic cycle analyses have demonstrated the benefits of using reheat in the turbine in order to increase specific power and thermal efficiency. Even better performance gains for specific power and thermal efficiency were predicted for power generation gas turbine engines when the turbine is coupled with a heat regenerator.

The report presents (1) the experimental investigation of combustion in a single-vane combustor, (2) the validation of the combustion model using single-vane combustor data, and (3) the investigation of *in situ* reheat for four- and five-stage industrial turbines. The numerical simulation proved that the combustion model is sufficiently accurate to produce reliable results for parametric studies. The numerical simulation showed that power could be increased by up to 5% with a modest amount of fuel injected in the turbine.

The numerical simulation showed that the best location for fuel injection is at the trailing edge of the inlet guide vane. The flow conditions at the trailing edge promote combustion because (1) the gas velocity in the airfoil's wake is small and (2) the vortices shed at the trailing edge enhance mixing of fuel and oxygen. Consequently, the trailing edge acts as a good flame holder. When the fuel was injected in the second or third stages, however, the combustion either was not initiated or was much weaker compared to the case when the fuel was injected at the inlet guide vane. Reduced temperature and pressure adversely affected *in situ* reheat on second and third vanes.

Fuel injection at the leading edge of the second vane did not significantly increase power, although a counter-flow flame had some advantages. The numerical simulation showed that the location of the injection at the leading edge must be moved toward the pressure side in order to avoid the flame being swept towards the suction side. The flow unsteadiness at leading edge was another factor that adversely affected the combustion of a fuel injected with constant velocity.

The most important next step is the experimental investigation of a scaled down, one and a half stage turbine-combustor. This experimental investigation will provide critical data on the interaction between the *in situ* reheat, the rotor/stator interaction and the combustor hot streaks. This experiment will also provide the apparatus necessary to investigate different approaches for fuel injection and blade cooling. The experiment can be done at the blow down facility of the Texas A&M University. This facility provides approximately 10 kg/sec at 44 bars for approximately 5 minutes. If necessary, the mass flow rate can be increased by reducing the operating time. A large variety of measurement equipment is also available, including Laser Doppler Anemometry, Particle Image Velocimetry, 18-hole omni-directional probes, etc.

For the numerical simulation, the next step should be the replacement of the quasi-three-dimensional model by a fully three-dimensional model, in order to capture the radial variation effects on *in situ* reheat. The modeling of the combustion process can be improved as well. One possible improvement is related to the diffusion modeling, where the constant diffusion coefficients will be replaced by binary mixture coefficients. Another improvement will be obtained by replacing the existing two-step combustion model by a five-step combustion model or, even better, by the ARM2 model, a sixteen-step combustion model.

1. INTRODUCTION AND BACKGROUND

Thermodynamic cycle analysis has demonstrated the benefits of using reheat in the turbine to increase specific power and thermal efficiency. Even better performance gains for specific power and thermal efficiency are predicted for power generation gas-turbine engines when the turbine is coupled with a heat regenerator. Starting in the 1960s, several patents have been awarded for inventions that address various aspects of turbine reheat.

In spite of these advances, the technological challenges and the difficulty of predicting and understanding the details of the transport phenomena inside the reheat turbine have precluded the development of turbine-combustors. Herein, a turbine-combustor is defined as a turbine in which fuel is injected and combustion takes place. The process of combustion in the turbine is called *in situ* reheat.

Several challenges are associated with combustion in the turbine-burner: mixed subsonic and supersonic flows; flows with large unsteadiness due to the rotating blades; hydrodynamic instabilities and large straining of the flow due to the very large three-dimensional acceleration and stratified mixtures. The obvious drawback associated with the strained flows in the turbine-burner is that widely varying velocities can result in widely varying residence times for different flow paths and as a result there are flammability difficulties for regions with shorter residence times. In addition, transverse variation in velocity and kinetic energy can cause variations in entropy and stagnation entropy that impact heat transfer. The heat transfer and mixing could be enhanced by increasing interface area due to strained flows.

The experimental investigation and numerical simulations performed in this study explore: (1) the validity of the combustion model on a simple combustion probe for which experimental data were generated, and (2) the influence of various fuel injection parameters on the performance of a turbine-combustor based on a gas turbine power plant. The parameters that were varied in this set of calculations are: (1) injection velocity, (2) fuel temperature, (3) injection hole size, (4) airfoil injection location, (5) injection row, and (6) direction of fuel injection velocity. The calculated output for each case includes the turbine-combustor power increase, the volume and mass fraction of the species, total temperature and enthalpy, and mixedness across the main stream of the total enthalpy and temperature (relative for rotors and absolute for stators) as well as mass fractions for CO and CH_4 .

2. GENERAL MODELING PROCEDURE

2.1 Physical Model

The flow and combustion through a multi-row turbine-burner with arbitrary blade counts is modeled by the Reynolds-averaged Navier-Stokes equations and the species conservation equations. To reduce the computational time of the *in situ* reheat in the multi-stage turbine-burner, the flow and combustion are modeled as quasi-three-dimensional. The calibration of the combustion model against the experimental data was done using two-dimensional and three-dimensional models. This section will present the details of the governing equations and the chemistry model.

2.2 Governing Equations

The unsteady, compressible flow through the turbine-combustor is modeled by the Reynolds-averaged Navier-Stokes equations. The flow is assumed to be fully turbulent and the kinematic viscosity is computed using Sutherland's law. The Reynolds-averaged Navier-Stokes equations and species conservation equations are simplified by using the thin-layer assumption.

In the hypothesis of unity Lewis number, both the Reynolds-averaged Navier-Stokes and species equations can be written as:

$$\frac{\partial Q}{\partial \tau} + \frac{\partial F}{\partial \xi} + \frac{\partial G}{\partial \eta} = \frac{\sqrt{\gamma_\infty} M_\infty}{Re_\infty} \frac{\partial S}{\partial \eta} + S_{ch}. \quad (1)$$

Note that equation (1) is written in the body-fitted curvilinear coordinate system (ξ, η, τ) .

The state and flux vectors of the Reynolds-averaged Navier-Stokes equations in the Cartesian coordinates are

$$q^{ns} = \begin{bmatrix} \rho \\ \rho u \\ \rho v \\ e \end{bmatrix}, \quad f^{ns} = \begin{bmatrix} \rho u \\ \rho u^2 + p \\ \rho uv \\ (e + p)u \end{bmatrix}, \quad g^{ns} = \begin{bmatrix} \rho v \\ \rho uv \\ \rho v^2 + p \\ (e + p)v \end{bmatrix}.$$

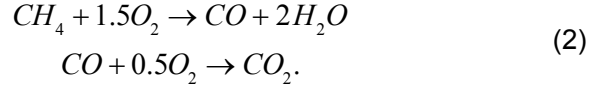
The state and flux vectors of the species conservation equations in the Cartesian coordinates are

$$q^{sp} = \begin{bmatrix} \rho y_1 \\ \rho y_2 \\ \mathbf{M} \\ \rho y_N \end{bmatrix}, \quad f^{sp} = \begin{bmatrix} \rho u y_1 \\ \rho u y_2 \\ \mathbf{M} \\ \rho u y_N \end{bmatrix}, \quad g^{sp} = \begin{bmatrix} \rho v y_1 \\ \rho v y_2 \\ \mathbf{M} \\ \rho v y_N \end{bmatrix}.$$

Further details on the description of the viscous terms and chemical source terms are presented in [2].

2.3 Chemistry Model

The chemistry model used herein to simulate the *in situ* reheat is a two-step, global, finite rate combustion model [3] for methane and combustion gases



The rate of progress (or Arrhenius-like reaction rate) for methane oxidation is given by:

$$q_1 = A_1 \exp(E_1 / R_M / T) [CH_4]^{-0.3} [O_2]^{1.3}, \quad (3)$$

where $A_1 = 2.8 \cdot 10^9 \text{ s}^{-1}$, $E_1 / R_M = 24360 \text{ K}$. The reaction rate for the CO / CO_2 equilibrium is:

$$q_2 = A_2 \exp(E_2 / R_M / T) [CO] [O_2]^{0.25} [H_2O]^{0.5} \quad (4)$$

with $A_2 = 2.249 \cdot 10^{12} \text{ (m}^3 / \text{kmol)}^{0.75} \text{ s}^{-1}$ and $E_2 / R_M = 20130 \text{ K}$. The symbols in the square brackets represent local molar concentrations of various species. The net formation/destruction rate of each species due to all reactions is:

$$W_i = \sum_{k=1}^{Nf} M_i v_{ik} q_k,$$

where v_{ik} are the generalized stoichiometric coefficients. Note that the generalized stoichiometric coefficient is $v_{ik} = v_{ik}'' - v_{ik}'$ where v_{ik}' and v_{ik}'' are stoichiometric coefficients for species i in reaction k appearing as reactant or as a product. Additional details on the implementation of the chemistry model can be found in [2].

2.4 Numerical Model

The numerical model used herein is based on an existing algorithm developed for unsteady flows in turbomachinery [1]. The Reynolds-averaged Navier-Stokes equations and the species equations are written in the strong conservation form. The fully implicit, finite-difference approximation is solved iteratively at each time level, using an approximate factorization method. Three Newton-Raphson sub-iterations are used to reduce the linearization and factorization errors at each time step. The convective terms are evaluated using a third-order accurate upwind-biased Roe scheme. The viscous terms are evaluated using second-order accurate central differences. The scheme is second-order accurate in time.

2.5 Grid Generation

The computational domain used to simulate the flow inside the turbine-combustor is reduced by taking into account flow periodicity. Two types of grids are used to

discretize the flow field surrounding the rotating and stationary airfoils, as shown in Figure 17. An O-grid is used to resolve the governing equations near the airfoil, where the viscous effects are important. An H-grid is used to discretize the governing equations away from the airfoil. The O-grid is generated using an elliptical method. The H-grid is algebraically generated. The O- and H-grids are overlaid. The flow variables are communicated between the O- and H-grids through bilinear interpolation. The H-grids corresponding to consecutive rotor and stator airfoils are allowed to slip past each other to simulate the relative motion.

2.6 Discretization of Governing Equations

The transport of chemical species is modeled by the mass, momentum, energy and species balance equations. These gas-dynamics and chemistry governing equations are solved herein using a fully decoupled implicit algorithm. Further discussions on the coupled vs. decoupled algorithms for combustion problems can be found in [2]. A correction technique has been developed to enforce the balance of mass fractions. The governing equations are discretized using an implicit, approximate-factorization, finite difference scheme in delta form. The discretized operational form of both the Reynolds-averaged Navier-Stokes (RANS) and species conservation equations, combined in a Newton-Raphson algorithm, is:

$$\left[I + \frac{\Delta\tau}{\Delta\xi} \left(\Delta_\xi (A^-)^p + \nabla_\xi (A^+)^p \right) \right] \left[I + \Delta\tau \frac{\hat{c}}{\rho_\infty} \sqrt{\frac{\rho_\infty}{p_\infty}} C_{i,j}^p + \frac{\Delta\tau}{\Delta\eta} \left(\Delta_\eta (B^-)^p + \nabla_\eta (B^+)^p - \frac{\sqrt{\gamma_\infty} M_\infty}{Re} \delta_\eta (Y)^p \right) \right] (Q_{i,j}^{p+1} - Q_{i,j}^p) = - (1.5Q_{i,j}^p - 2.0Q_{i,j}^{p-1} + 0.5Q_{i,j}^{p-2}) - \frac{\Delta\tau}{\Delta\xi} (\hat{F}_{i+\frac{1}{2},j}^p - \hat{F}_{i-\frac{1}{2},j}^p) - \frac{\Delta\tau}{\Delta\eta} (\hat{G}_{i,j+\frac{1}{2}}^p - \hat{G}_{i,j-\frac{1}{2}}^p) + \sqrt{\gamma_\infty} M_\infty Re^{-1} \frac{\Delta\tau}{\Delta\eta} (S_{i+\frac{1}{2},j}^p - S_{i-\frac{1}{2},j}^p) + (S_{ch}^p)_{i,j} \quad (5)$$

where A and B are the flux Jacobian matrices $A = \partial F / \partial Q$, $B = \partial G / \partial Q$. The Y and C matrices are $Y = \partial S / \partial Q$ and $C = \partial S_{ch} / \partial Q$. Note that the flux Jacobian matrices are split into $A = A^+ + A^-$, where $A^\pm = P \Lambda^\pm P^{-1}$. Λ is the spectral matrix of A , and P is the modal matrix of A . The spectral matrix Λ is split into $\Lambda = \Lambda^+ + \Lambda^-$, where the components of Λ^+ and Λ^- are $\lambda_i^- = 0.5(\lambda_i - |\lambda_i|)$ and $\lambda_i^+ = 0.5(\lambda_i + |\lambda_i|)$, respectively. The same flux vector splitting approach is applied to the matrix B . In equation (5), Δ , ∇ and δ are forward, backward and central differences operators, respectively. Q^p is an approximation of Q^{n+1} . At any time step n , the value of Q^p varies from Q^n at first internal iteration when $p = 0$, to Q^{n+1} when integration of equation (5) has converged. Additional details on the implementation of the inter-cell numerical fluxes and on the Roe's approximate Riemann solver are presented in [2].

2.7 Boundary Conditions

Two classes of boundary conditions must be enforced on the grid boundaries: (1) natural boundary conditions, and (2) zonal boundary conditions. The natural boundaries include inlet, outlet, periodic and the airfoil surfaces. The zonal boundaries include the patched and overlaid boundaries.

The inlet boundary conditions include the specification of the flow angle, average total pressure and downstream propagating Riemann invariant. The upstream propagating Riemann invariant is extrapolated from the interior of the domain. At the outlet, the average static pressure is specified, while the downstream propagating Riemann invariant, circumferential velocity, and entropy are extrapolated from the interior of the domain. Periodicity is enforced by matching flow conditions between the lower surface of the lowest H-grid of a row and the upper surface of the top most H-grid of the same row. At the airfoil surface, the following boundary conditions are enforced: the “no slip” condition, the adiabatic wall condition, and the zero normal pressure gradient condition.

For the zonal boundary conditions of the overlaid boundaries, data are transferred from the H-grid to the O-grid along the O-grid’s outermost grid line. Data are then transferred back to the H-grid along its inner boundary. At the end of each iteration, an explicit, corrective, interpolation procedure is performed. The patch boundaries are treated similarly, using linear interpolation to update data between adjoining grids.

3. EXPERIMENTAL POINTS

This section presents the experimental data obtained for a single-vane burner operating at conditions similar to the inlet guide vane of a typical power generation turbine. Because of experimental limitations, the total pressure upstream of the combustion probe was smaller than the total pressure upstream of the inlet guide vane of a typical power generation turbine. These experimental data were compared against the numerical results corresponding to two-dimensional and three-dimensional models. The comparison between the experimental data and the numerical results was done in order to validate the combustion model.

3.1 Approach

To verify the validity of the methane combustion model to *in situ* reheat applications, a single-vane burner was experimentally investigated and numerically simulated. In-situ reheat tests were run in the Siemens Westinghouse small-scale, full-pressure, combustion test facility, shown in Figure 1. Preheated air (0.20 kg/s) and natural gas were delivered to a low-NO_x burner section, which was run at full pressure (typically 14 bar). Air preheat temperature and fuel/air ratio were adjusted to give an exhaust gas stagnation temperature and composition corresponding to a selected location in a turbine cascade. The exhaust gas was then passed through a pressure-reducing orifice to increase the Mach number in the injection and sampling sections to typical turbine levels. A back pressure control valve was used to set the sampling section pressure.

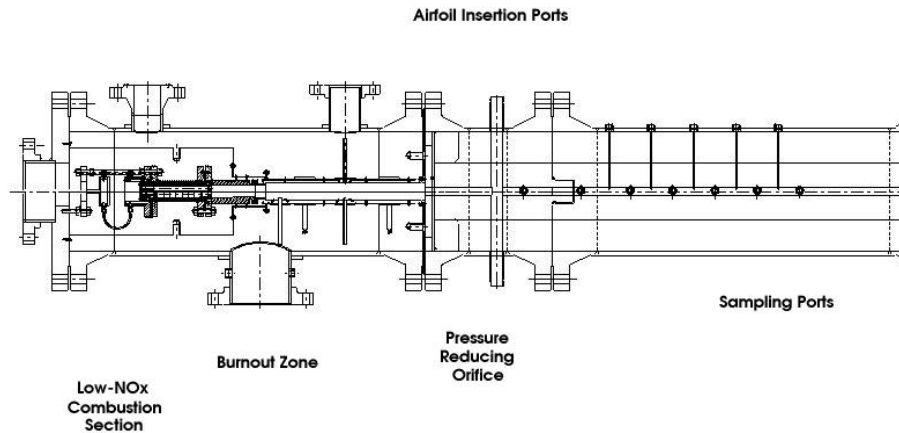
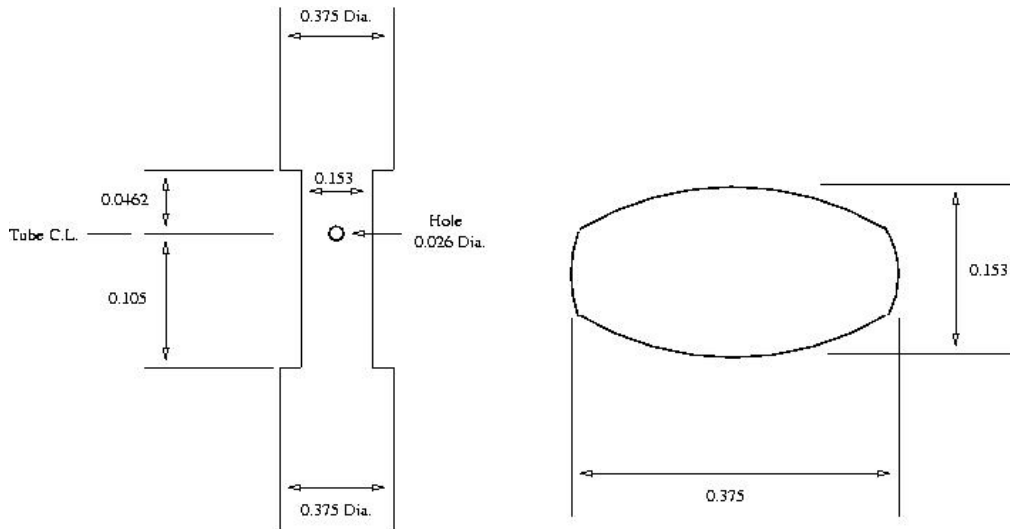


Figure 1 – Experimental apparatus.



NOTE: All Lengths Shown in Inches
 Drawing Not To Scale

Figure 2 – Combustion probe.

Air flow to the system was measured using a calibrated orifice plate, and natural gas flow with a mass flow controller with accuracies of 2 and 1 % respectively. Gases were sampled at various locations downstream of the injection point, and compositions determined using a gas chromatograph, with error limits of $\pm 5\%$.

The geometry of the combustion probe is shown in Figure 2. Fuel was injected through a 0.66 mm diameter hole. The probe was inserted into a 1.0 inch (2.54 cm) x 0.7 inch (1.78 cm) channel, which necked down to a 0.7 x 0.7 channel immediately downstream. Temperature and gas composition were measured at several locations downstream of the fuel injector. Tests simulating vane 1 trailing edge injection produced complete burnout at the first sample location. Two flow cases are presented herein: 3B1 (Blade 1 trailing edge conditions) and 4B2 (Vane 2 trailing edge conditions). The flow parameters were calculated first for the probe without fuel injection. This simulation provided the static pressure value at the fuel injection location. Consequently, it was assumed that static pressure at fuel injection location was equal in the cases with and without fuel injection. The fuel density was calculated knowing the pressure, temperature and fuel composition. The injection velocity was the same as in the experimental investigation.

3.1.1 Case 3B1

Fuel was injected in a gas mixture that had a total pressure of 6.26 bar and total temperature of 1507 K. The mass flow rate of gas mixture upstream of the injector was 0.1345 kg/s. The composition of this gas mixture is given in Table 1.

CO ₂	4.84
H ₂ O	10.59
N ₂	73.48
O ₂	10.21
Ar	0.88

Table 1 – Gas mixture molar composition %, case 3B1

The composition of the injection fuel is given in Table 2. In the numerical simulation it was assumed that the fuel injected was pure CH₄. The temperature of the fuel was 289 K and the mass flow rate was 0.416 g/s. The static pressure at the exit from the 0.7 in x 0.7 in tube was 4.6 bar.

CH ₄	96.1
C ₂ H ₆	2.0
C ₃ H ₈	0.9
CO ₂	0.5
N ₂	0.5

Table 2 – Injection fuel molar composition %, case 3B1

3.1.2 Case 4B2

Fuel was injected in a gas mixture that had a total pressure of 6.27 bar and total temperature of 1336 K. The mass flow rate of gas mixture downstream of the injector was 0.1542 kg/s. The composition of the gas mixture at inlet in the 1 in x 0.7 in tube is given in Table 3.

CO ₂	4.36
H ₂ O	9.64
N ₂	73.85
O ₂	11.27
Ar	0.88

Table 3 – Gas mixture molar composition %, case 4B2

The composition of the injection fuel is given in Table 4. In the numerical simulation it was assumed that the fuel injected was pure CH₄. The temperature of the fuel was 289 K and the mass flow rate was 0.528 g/s. The static pressure at the exit from the 0.7 in x 0.7 in tube was 4.6 bar.

CH ₄	96.1
C ₂ H ₆	2.0
C ₃ H ₈	0.9
CO ₂	0.5
N ₂	0.5

Table 4 – Injection fuel molar composition %, case 4B2

3.2 TWO-DIMENSIONAL MODEL

3.2.1 Case 3B1

The parameters at fuel injection location are: temperature, $T = 289$ K, pressure, $p = 5.84$ bar, molecular mass, $M = 16.24$ kg/kmol, fuel density, $\rho = 3.948$ kg/m³, and velocity, $V = 308$ m/s. The three-dimensional effects of the flow and combustion downstream of the injector are important. The numerical simulation presented in this section was, however, two-dimensional. Three cases were considered in the numerical simulation: (1) the length of the injector equal to the diameter of the hole,

that is, 0.66 mm, (2) the length of the injector equal to the area of the hole from the experiment divided by the height of the tube (0.7 in), that is, 0.019 mm, and (3) the length of the injector equal to the geometrical average of the lengths used in cases (1) and (2). A good two-dimensional approximation of the three-dimensional solution should be situated in between the extreme values of the injector lengths. Note that the small length injector is just a model and not an engineering solution.

Large Injector Length

In the two-dimensional simulation, the length of the injector hole was equal to the diameter of the hole, that is, 0.66 mm. As a result, the ratio of inlet gases and fuel injection mass flow rates is larger than the actual value in the three-dimensional case. The mass flow rate of fuel per unit length is 0.802 kg/s.

Parameter	Experimental	Centerline	Area-weighted average	Mass-weighted average
CH_4	0.35	22.97	14.51	16.53
CO	0.16	0.10	0.13	0.14
CO_2	N.A.	4.55	6.69	6.24
O_2	N.A.	5.62	2.89	3.45
H_2O	N.A.	9.71	14.22	13.32

Table 5 – Species mole fraction % at 0.311 m downstream for case 3B1 while using large size injector

Parameter	Experimental	Centerline	Area-weighted average	Mass-weighted average
CH_4	0.08	19.00	15.38	15.95
CO	0.27	0.059	0.063	0.068
CO_2	N.A.	5.98	7.21	7.04
O_2	N.A.	3.47	1.69	1.95
H_2O	N.A.	12.68	15.10	14.75

Table 6 – Species mole fraction % at 0.654 m downstream for case 3B1 while using large size injector

	0.311 m	0.654 m	0.836 m
Centerline			
Static Temperature [K]	1159	1408	1512
Total Temperature [K]	1204	1474	1578
Area-weighted average			
Static Temperature [K]	1680	1716	1744
Total Temperature [K]	1716	1760	1794
Mass-weighted average			
Static Temperature [K]	1572	1671	1718
Total Temperature [K]	1608	1718	1770

Table 7 – Temperature values for large size injector, case 3B1. Experimental value at 0.836 m is 1478 K.

Small Injector Length

In the two-dimensional simulation, the length of the injector hole was equal to the area of the injector hole from the experiment divided by the height of the tube (0.7 in), that is, 0.019 mm. As a result, the ratio between the inlet gases and fuel injection mass flow rates is larger than the actual value in the three-dimensional case. The mass flow rate of fuel per unit length is 0.023 kg/s.

Parameter	Experimental	Centerline	Area-weighted average	Mass-weighted average
CH_4	0.35	0.0	1.11e-03	1.17e-03
CO	0.16	0.016	6.52e-03	6.87e-03
CO_2	N.A.	5.97	5.68	5.70
O_2	N.A.	7.46	8.20	8.16
H_2O	N.A.	12.75	12.27	12.30

Table 8 – Species mole fraction % at 0.311 m downstream for case 3B1 using small size injector

Parameter	Experimental	Centerline	Area-weighted average	Mass-weighted average
CH_4	0.08	0.00	1.29e-06	1.40e-06
CO	0.27	0.00	1.47e-05	1.60e-05
CO_2	N.A.	5.73	5.71	5.71
O_2	N.A.	7.97	8.16	8.15
H_2O	N.A.	12.31	12.31	12.31

Table 9 – Species mole fraction % at 0.654 m downstream for case 3B1 using small size injector

	0.311 m	0.654 m	0.836 m
Centerline			
Static Temperature [K]	1682	1621	1621
Total Temperature [K]	1745	1698	1698
Area-weighted average			
Static Temperature [K]	1622	1619	1620
Total Temperature [K]	1677	1679	1683
Mass-weighted average			
Static Temperature [K]	1625	1620	1621
Total Temperature [K]	1682	1682	1686

Table 10 – Temperature values for small size injector, case 3B1. Experimental value at 0.836 m is 1478 K.

Medium Injector Length

The injection length was the geometrical average between the large and small injectors used in the previous sections. As a result, the injector length was equal to 0.112 mm. The mass flow rate of fuel per unit length is 0.133 kg/s.

Parameter	Experimental	Centerline	Area-weighted average	Mass-weighted average
CH_4	0.35	0.0	0.15	0.15
CO	0.16	0.75	0.35	0.35
CO_2	N.A.	8.45	7.82	7.84
O_2	N.A.	0.61	2.85	2.80
H_2O	N.A.	19.07	17.18	17.22

Table 11 – Species mole fraction % at 0.311 m downstream for case 3B1 using the medium size injection

Parameter	Experimental	Centerline	Area-weighted average	Mass-weighted average
CH_4	0.08	0.0	5.15e-04	5.59e-04
CO	0.27	0.0	3.37e-03	3.65e-03
CO_2	N.A.	8.62	8.34	8.36
O_2	N.A.	1.63	2.36	2.31
H_2O	N.A.	18.09	17.53	17.57

Table 12 – Species mole fraction % at 0.654 m downstream for case 3B1 using the medium size injection.

	0.311 m	0.654 m	0.836 m
Centerline			
Static Temperature [K]	2208	2168	2109
Total Temperature [K]	2278	2257	2196
Area-weighted average			
Static Temperature [K]	2055	2104	2102
Total Temperature [K]	2112	2170	2172
Mass-weighted average			
Static Temperature [K]	2059	2108	2104
Total Temperature [K]	2118	2177	2175

Table 13 – Temperature values for medium size injector, case 3B1. Experimental value at 0.836 m is 1478 K.

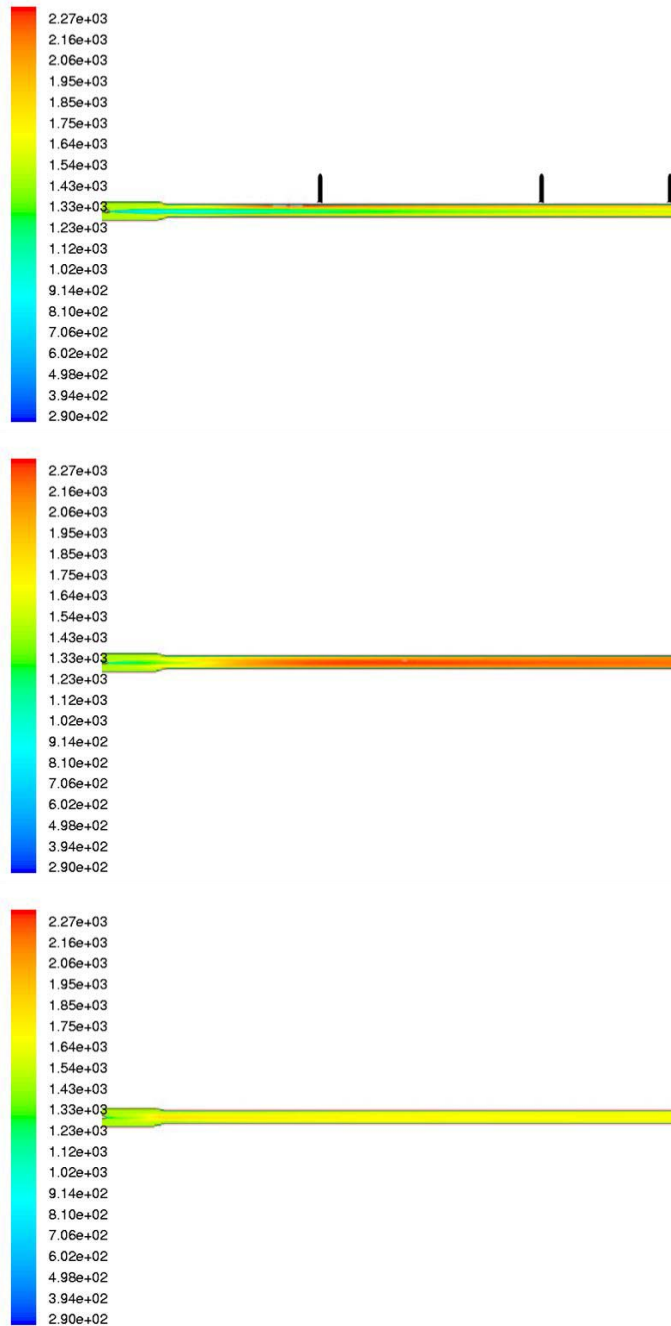


Figure 3 – Total temperature contours for case 3B1. Top: large width, middle: medium width, bottom: small width injector.

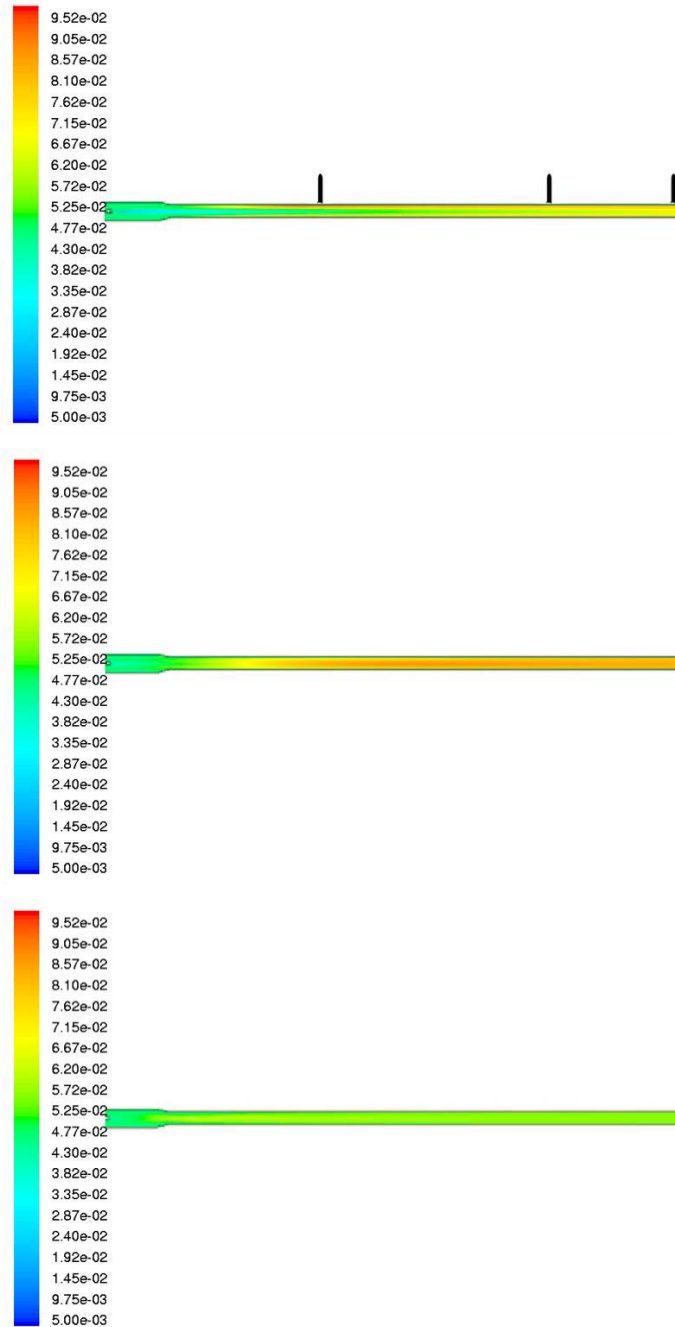


Figure 4 –Mole fraction contours for case 3B1. Top: large width, middle: medium width, bottom: small width injector.

The larger injector introduced too much fuel and combustion conditions existed only along the walls. Most of the middle portion of the tube did not react. Consequently, not all the fuel was burned, as shown in Figure 5.

The medium injector produced the largest temperature increase. The flame was situated in the middle of the tube. All the methane was burned, as shown in Figure 5.

The small injector produced the smallest temperature increase. The flame was situated at the inlet in the sample section, that is, the 0.7 in by 0.7 in tube. All the methane was burned upstream of the 0.311 m location, as shown in Figure 5.

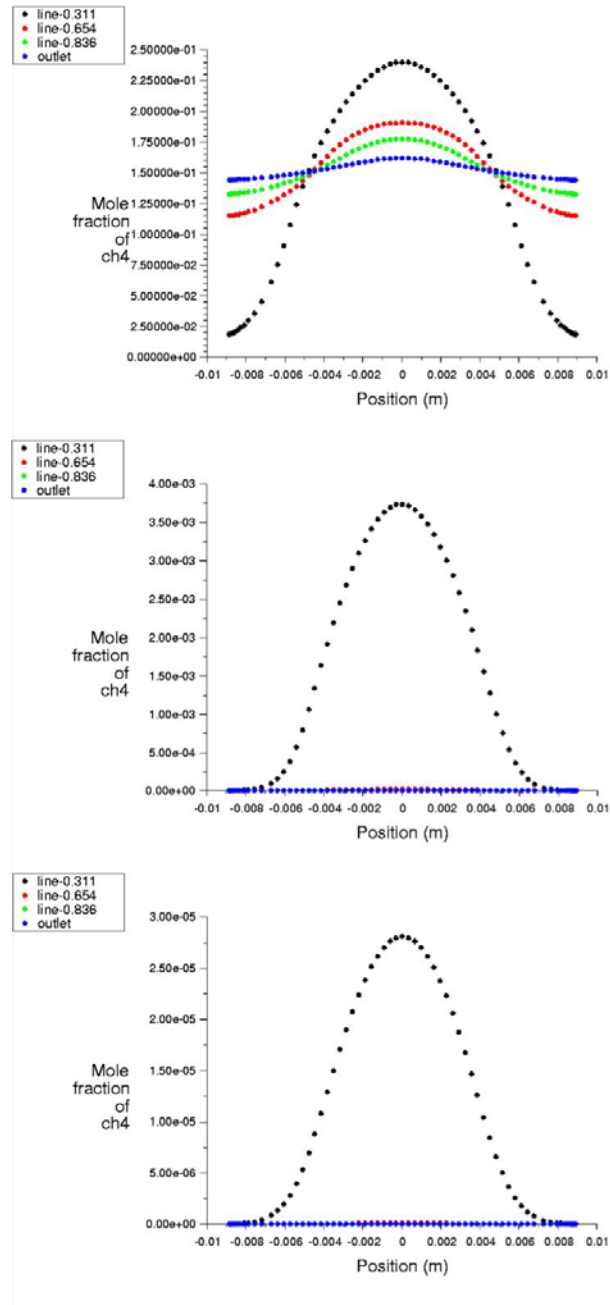


Figure 5 – Methane mole fraction at several locations along the sample section. Top: large width, middle: medium width, bottom: small width injector.

3.2.2 Case 4B2

The parameters at fuel injection location are: temperature, $T = 289$ K, pressure, $p = 5.79$ bar, molecular mass, $M = 16.24$ kg/kmol, fuel density, $\rho = 3.914$ kg/m³, and velocity, $V = 394.3$ m/s. Two cases were considered in the numerical simulation: (1) the length of the injector equal to the diameter of the hole, that is, 0.66

mm, and (2) the length of the injector equal to the area of the hole from the experiment divided by the height of the tube (0.7 in), that is, 0.019 mm. A good two-dimensional approximation of the three-dimensional solution is situated in between the two injector lengths. Note that the small length injector is just a model and not an engineering solution.

Large Injector Length

The length of the injector in this case was equal to the diameter of the injector hole, that is, 0.66 mm. The mass flow rate of fuel per unit length is 1.018 kg/s.

Parameter	Experimental	Centerline	Area-weighted average	Mass-weighted average
CH_4	0.45	16.00	15.43	15.50
CO	0.17	0.02	0.02	0.02
CO_2	N.A.	3.76	3.84	3.84
O_2	N.A.	9.07	9.22	9.21
H_2O	N.A.	8.17	8.35	8.34

Table 14 – Species mole fraction % at 0.765 m downstream for case 4B2

Parameter	Experimental	Centerline	Area-weighted average	Mass-weighted average
CH_4	0.41	15.00	15.49	15.50
CO	0.18	0.019	0.019	0.02
CO_2	N.A.	3.79	3.85	3.84
O_2	N.A.	9.19	9.21	9.21
H_2O	N.A.	8.27	8.35	8.34

Table 15 – Species mole fraction % at 1.059 m downstream for case 4B2

	0.765 m	0.840 m	1.059 m
Centerline			
Static Temperature [K]	1049	1049	1059
Total Temperature [K]	1108	1108	1129
Area-weighted average			
Static Temperature [K]	1078	1076	1071
Total Temperature [K]	1126	1126	1125
Mass-weighted average			
Static Temperature [K]	1076	1075	1071
Total Temperature [K]	1125	1126	1126

**Table 16 – Temperature values at requested locations for case 4B2.
Experimental value at 0.84 m is 1252 K.**

Small Injector Length

The length of the injector in this case was equal to the area of the injector hole from the experiment divided by the height of the tube (0.7 in), that is, 0.019 mm. The mass flow rate of fuel per unit length is 0.029 kg/s.

Parameter	Experimental	Centerline	Area-weighted average	Mass-weighted average
CH_4	0.45	0.0	1.58e-04	1.73e-04
CO	0.17	2.7e-03	1.02e-03	1.12e-03
CO_2	N.A.	5.31	5.30	5.31
O_2	N.A.	8.96	9.11	9.10
H_2O	N.A.	11.57	11.51	11.52

Table 17 – Species mole fraction % at 0.765 m downstream for case 4B2

Parameter	Experimental	Centerline	Area-weighted average	Mass-weighted average
CH_4	0.41	0.0	2.71e-07	2.95e-07
CO	0.18	0.0	3.25e-06	3.54e-06
CO_2	N.A.	05.31	05.31	05.31
O_2	N.A.	09.07	09.10	09.10
H_2O	N.A.	11.45	11.51	11.52

Table 18 – Species mole fraction % at 1.059 m downstream for case 4B2

	0.765 m	0.840 m	1.059 m
Centerline			
Static Temperature [K]	1467	1467	1454
Total Temperature [K]	1543	1543	1543
Area-weighted average			
Static Temperature [K]	1467	1465	1460
Total Temperature [K]	1532	1532	1532
Mass-weighted average			
Static Temperature [K]	1467	1466	1460
Total Temperature [K]	1534	1534	1534

Table 19 – Temperature values at requested locations for case 4B2. Experimental value at 0.84 m is 1252 K.

3.3 Three-Dimensional Model

This section presents the validation of the combustion model against the experimental data for a single-vane burner using a three-dimensional flow and combustion model.

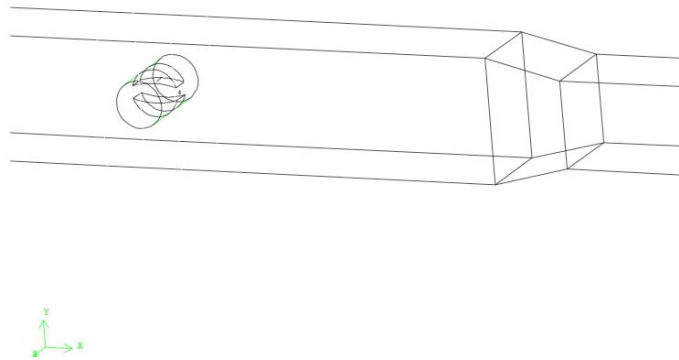


Figure 6 –Detail of the computational domain of the single-vane burner.

The computational domain extended 0.115 m upstream from the vane injection location and 1.071 m downstream. A detail of the computational domain is shown in Figure 6. The shape of the vane burner was defined by the intersection of two radii. The injection hole had a diameter of 0.66 mm . The injection hole was located at the center of the pipe, however, the shoulders of the vane were not equally-spaced with respect to the injection hole. A detail of the computational grid of the single-vane burner is shown in Figure 7.

Wall functions were utilized to reduce the number of grid points in the boundary layer regions. Consequently, the number of grid cells was limited to approximately 2.2 million. The grid is unstructured and was generated with Gambit.

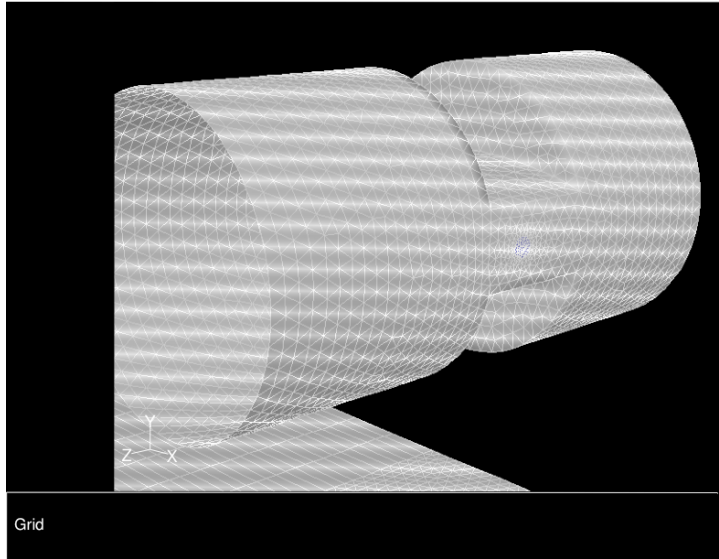


Figure 7 – Detail of the single-vane burner grid.

The chemistry model used to simulate the *in situ* reheat was the two-step finite rate combustion model for methane and combustion gases described by equations 2 and 3. The flow and combustion in the single-vane burner were modeled with Fluent as opposed to the four-stage turbine-burner which was modeled with the CoRSI code described in the previous sections. Both Fluent and CoRSI codes had an identical chemistry model.

At the inlet in the computational domain, upstream from the injection vane, the input data specified total pressure, initial static pressure, total temperature, turbulence intensity, hydraulic diameter, and the composition of the gas mixture, as shown in Table 20. The input data at the injector location specified the same list of variables as at inlet. The values of these variables are also shown in Table 20. Note that the small quantities of ethane and propane were lumped into methane in order to be able to use the two-reaction model presented above. The mass fraction of N_2 is not an input data for the problem. The value of the N_2 is calculated such that the sum of all mass fraction species equals 1. At the outlet, the static pressure value of 4.6 *bar* was specified.

Parameter	Inlet	Injection
Total pressure [<i>bar</i>]	6.26	7.95
Initial static pressure [<i>bar</i>]	5.93	5.84
Total temperature [<i>K</i>]	1507	311
Turbulence intensity [%]	10	10
Hydraulic diameter [<i>m</i>]	0.0254	0.00066
Mass fraction		
CH_4	0.0	0.9778
O_2	0.115	0.0
CO_2	0.0754	0.01355
CO	0.0	0.0
H_2O	0.06755	0.0
N_2	0.74205	0.00865

Table 20 – Input data for the vane-burner.

The results shown herein illustrate the spatial variation of methane, CO_2 and total temperature. Figure 8 shows the variation of methane along the $z=0$ plane of the combustor and at four planes perpendicular to the x -axis located at 12, 15, 20 and 35 *mm* downstream of the injector. The methane completely burned at approximately 70 *mm* downstream of the injector. Figure 9 shows methane variation in the four planes described above. The lack of symmetry of the methane contour plots is due to the slightly off-center position of the vane. All other variables show a similar lack of symmetry.

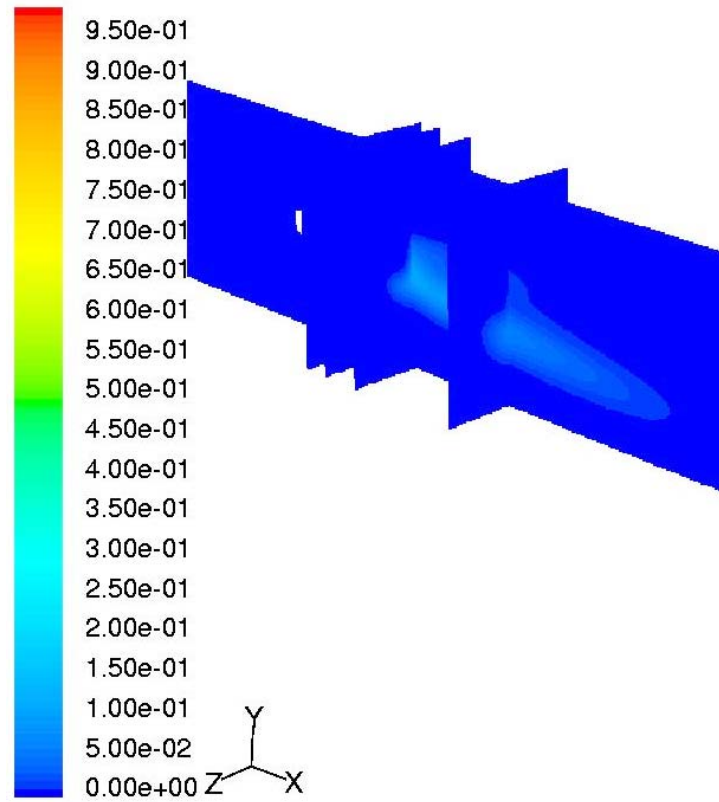


Figure 8 – Contour plots of methane.

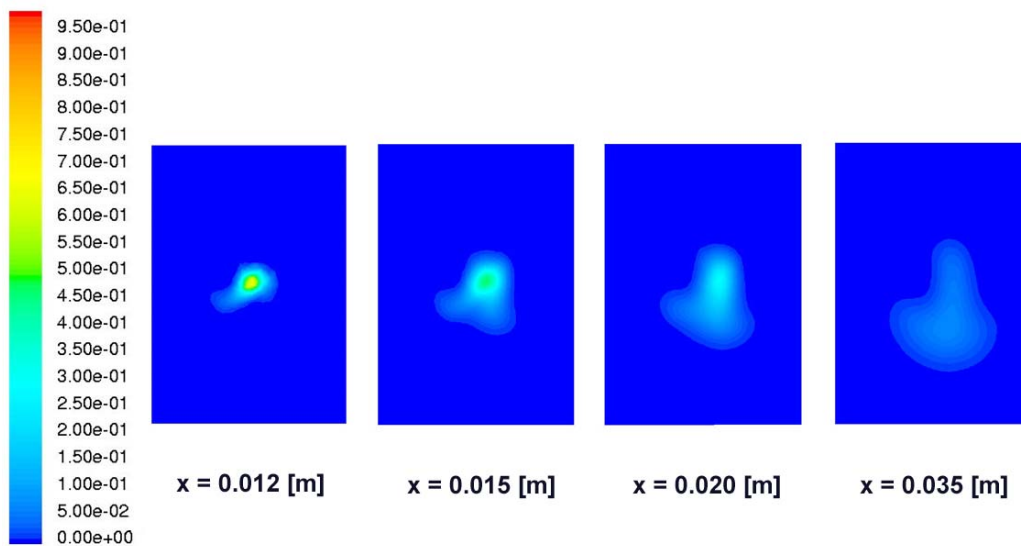


Figure 9 – Contour plots of methane at x =constant planes.

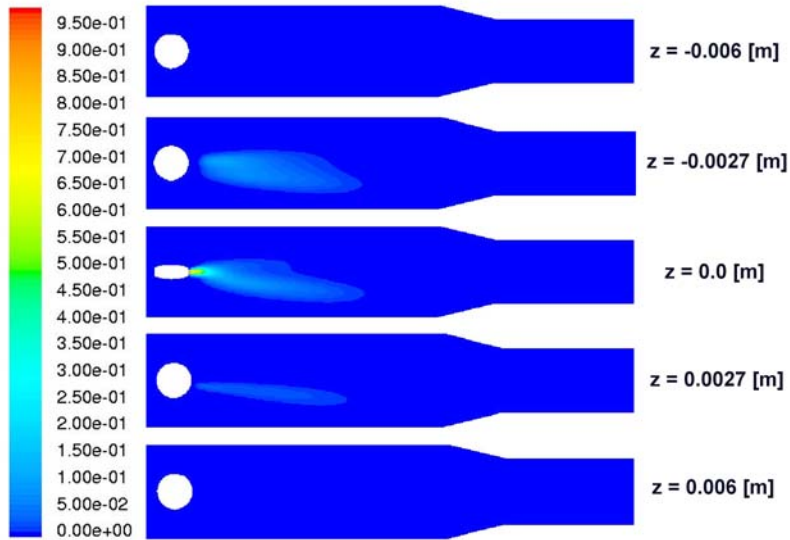


Figure 10 – Methane mole fraction z -plane contour plots. The $z = 0.0$ is the same as shown in Figure 8.

Figure 11 shows the variation of CO along the $z=0$ plane of the combustor and at five planes perpendicular to the x -axis located at 12, 35, 45, 79 and 94 mm downstream of the injector. The flame is off-center and closer to the lower wall. Figure 12 shows CO variation in the five planes described above. Note that the last plane, located at 94 mm downstream of the injector, is situated in the smaller section of the pipe (0.7 in by 0.7 in).

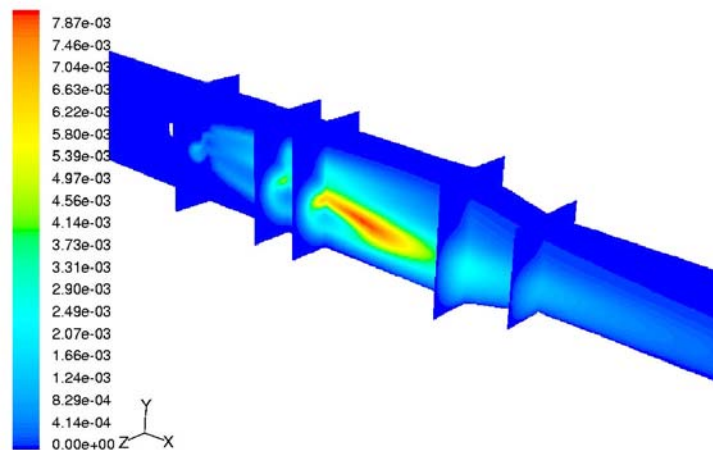


Figure 11 – Contour plots of CO .

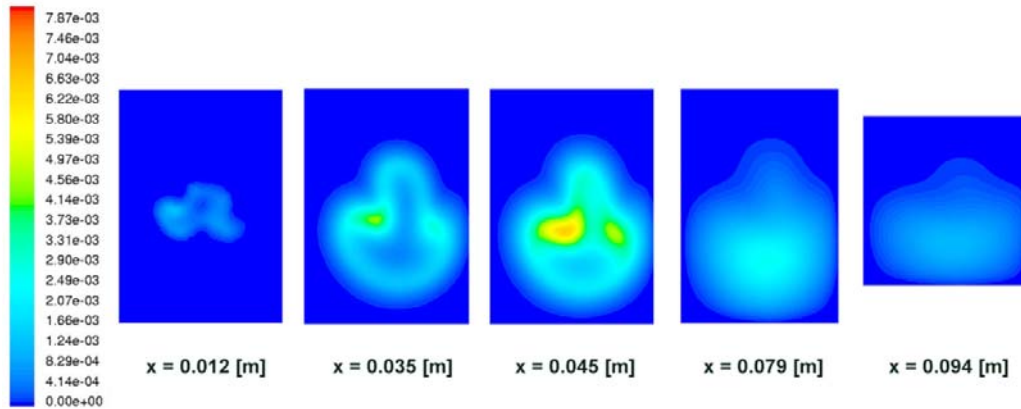


Figure 12 – Contour plots of CO at x =constant planes.

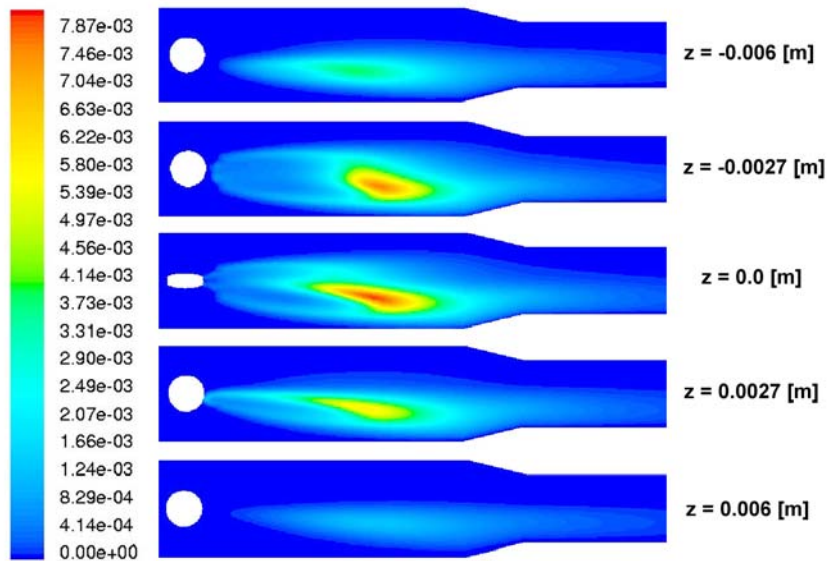


Figure 13 – Carbon monoxide mole fraction z -plane contour plots. The $z = 0.0$ is the same as shown in Figure 11.

Figure 14 shows the variation of total temperature along the $z=0$ plane of the combustor and at five planes perpendicular to the x -axis located at 12, 35, 79, 94 and 120 mm downstream of the injector. The maximum total temperature is approximately 1970 K . Figure 15 shows total temperature variation in the five planes described above. The static temperature predicted by the numerical simulation at the centerline at 836 mm downstream of the injector is 1536 K . The measured temperature at the same location is 1478 K . The predicted temperature is 58 K higher than the measured temperature. There are several possible reasons for the temperature difference, such as: (1) simplified kinetic scheme, (2) limitations of the turbulence model, and (3) limitations due to using binary diffusion coefficients. In our opinion, the most important (and likely) reason for the 58K temperature difference is the use of adiabatic boundary conditions that neglected the heat transfer at the wall surface. The gas chromatograph found small traces of CH_4 (0.35%) and CO (0.16%) at 0.311 m downstream of the injector. The numerical simulation predicted

values close to zero (smaller than 10^{-4} %) for both CH_4 and CO at the same location.

The numerical simulation was done on an IBM Regatta pSeries 690 computer using 4 processors. The computation converged in approximately 3,500 iterations. The wall clock time for this run was approximately 195 hours.

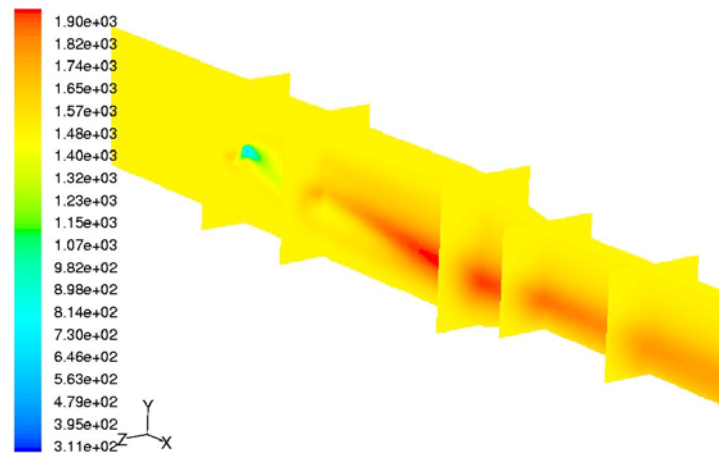


Figure 14 – Contour plots of total temperature.

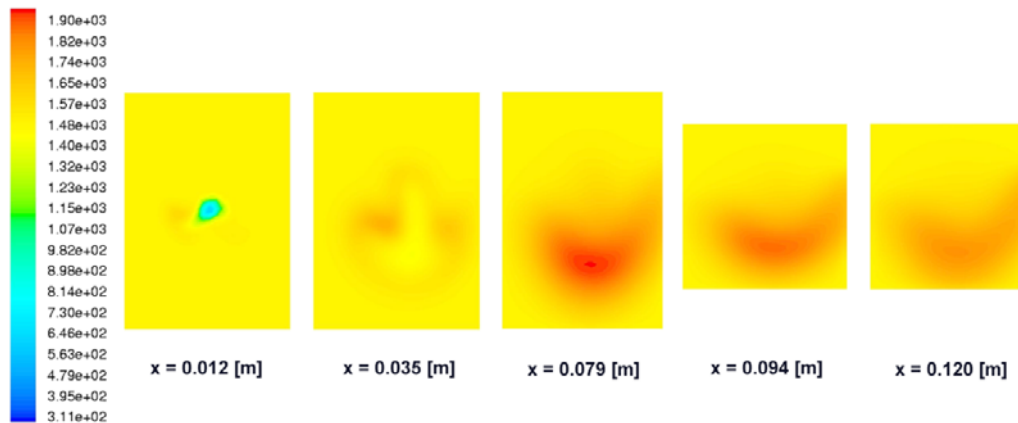


Figure 15 – Contour plots of total temperature at x =constant planes.

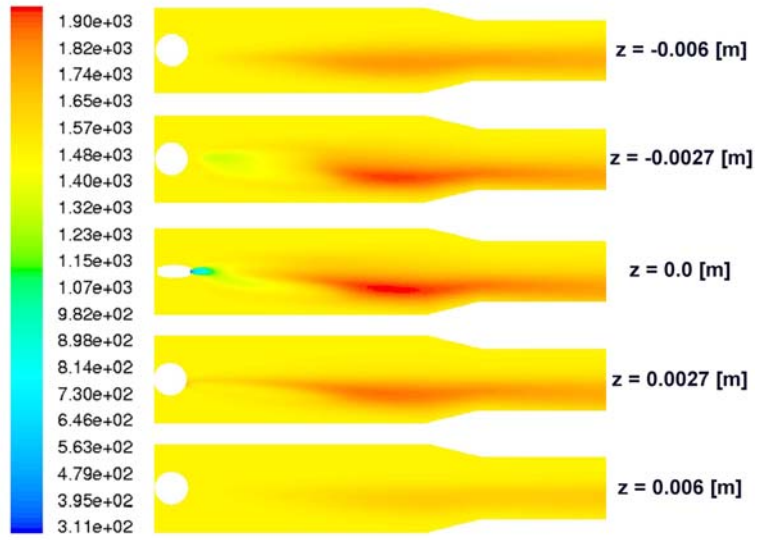


Figure 16 – Total temperature z-plane contour plots. The z = 0.0 is the same as shown in Figure 14.

4. INDUSTRIAL GAS TURBINE SIMULATION

This section presents the numerical simulation of *in situ* reheat in four- and a five-stage large industrial gas turbines. The numerical simulation included both *in situ* reheat cases and a case without combustion. The flow in the turbine without combustion was simulated first in order to provide reference values, particularly the power and the fuel injection pressure at the trailing edge of the inlet guide vane. The simulations use blade path dimensions and shapes representative of a large industrial gas turbine.

4.1 Approach

Once the combustion model was validated for the single-vane burner, the next step was to investigate a four-stage turbine-burner. The purpose of this numerical investigation was to determine the influence of several fuel injection parameters on the flow and combustion in the turbine-burner. Since the computational time of a three-dimensional model for the four-stage turbine-burner would exceed the computational time of the single-vane burner by a factor of four, and since a parametric analysis of the turbine-burner was necessary, it was decided to replace the three-dimensional model by a less computational expensive quasi-three-dimensional model. A quasi-three-dimensional, as opposed to a two-dimensional model, was needed in order to take into account the large radial variation of the four-stage turbine. Since Fluent does not have a quasi-three-dimensional model, the CoRSI code was used instead.

4.2 Geometry and Flow Conditions

The blade count of the four-stage turbine-combustor required a full-annulus simulation for a dimensionally accurate computation. To reduce the computational effort, it was assumed that there were an equal number of airfoils in each turbine row. As a result, all airfoils except for the inlet guide vane airfoils were rescaled by factors equal to the number of airfoils per row divided by the number of airfoils per row one. An investigation of the influence of airfoil count on the turbine flow showed that the unsteady effects were amplified when a simplified airfoil count 1:1 was used [1]. Consequently, the results obtained using the simplified airfoil count represent an upper limit for the unsteady effects.

4.3 Accuracy of Numerical Results

To validate the accuracy of the numerical results corresponding to the governing equations used, it was necessary to show that the results were independent of the grid which discretizes the computational domain. The verification of grid independence results was presented in [2], where a one-stage turbine-combustor was simulated. Note that the grids were generated such that, for the given flow conditions, the y^+ number was less than 1. Approximately 20 grid points were used to discretize the boundary layer regions.

Based on the conclusions of accuracy investigation presented in [2], the medium grid was used herein since it provided the best compromise between accuracy and computational cost. This grid had 53 grid points normal to the airfoil and 225 grid points along the airfoil in the O-grid, and 75 grid points in the axial direction and 75 grid points in the circumferential direction in the H-grid. The stator airfoils and rotor airfoils had the same number of grid points. The inlet and outlet H-grids each had 36

grid points in the axial direction and 75 grid points in the circumferential direction. The grid is shown in Figure 17, where for clarity every other grid point in each direction is shown.

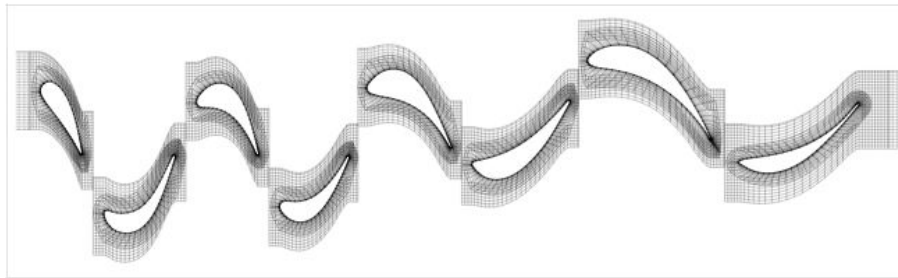


Figure 17 – Detail of the medium grid (every other grid point in each direction shown).

The results presented in this report were computed using three Newton sub-iterations per time-step and 3000 time-steps per cycle. Here, a cycle is defined as the time required for a rotor to travel a distance equal to the pitch length at mid-span. To ensure time-periodicity, each simulation was run in excess of 80 cycles. The numerical simulations were run on a 64-processor SGI Origin 3800 computer, a 32-processor IBM Regatta pSeries 690 computer and a Power Mac G5 computer. The computational time for a cycle was approximately 2.5 hours on a Power Mac G5 computer. Approximately 50 cycles are necessary to obtain a converged solution.

4.4 Run Set 1

The species mass fractions of the gas mixture at the inlet were:

$$X_{CH_4} = 0.0$$

$$X_{CO_2} = 0.0775$$

$$X_{CO} = 5.979 \times 10^{-6}$$

$$X_{H_2O} = 0.0680$$

$$X_{N_2} = 0.7288$$

$$X_{O_2} = 0.1131$$

$$X_{Ar} = 0.0124$$

$$X_{H_2} = 2.536 \times 10^{-7}$$

for all cases with and without combustion. The inlet flow parameters were: the static temperature $T_{-\infty} = 1840$ K, the static pressure $p_{-\infty} = 18.6621$ bar, the axial Mach number $M_{-\infty} = 0.1528$ and the inlet flow was axial. The resulting inlet Reynolds number based on the first vane axial chord was $Re_{-\infty} = 825,235$. At the exit, the static pressure p_{exit} was imposed through the ratio $p_{exit} / p_{-\infty}^* = 0.054$, where $p_{-\infty}^*$ is the total inlet pressure. The turbine speed was equal to 3,600 rpm and the stream surface for the two-dimensional calculations was taken at the midspan radius of 1.025 m. The stream tube thickness variation was considered in order to incorporate quasi-three-

dimensional effects. The mass flow rate of gases at turbine inlet was 88.085×10^{-3} kg/s per vane and per mm of vane span.

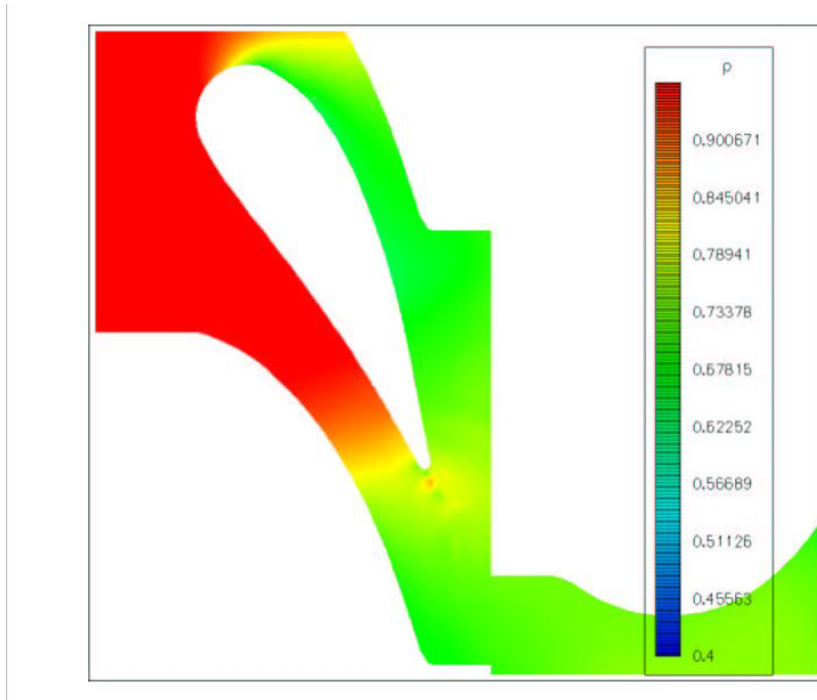


Figure 18 – Static pressure on first row of vanes in the case without combustion.

The base case for the fuel injection simulations is designated as C1Y and involves a low temperature, low fuel flow injection of pure methane at the trailing edge of each vane in the first row, with a jet oriented along its chord. At the injection hole the imposed static temperature, injection velocity and methane mass concentration were $T_{hole} = 313$ K, $V_{hole} = 77.32$ m/s and $X_{CH_4} = 1.0$, respectively. An equivalent hole width of 0.55 mm was considered which is the physical hole width corrected for the injection velocity nonuniformity. The static pressure at fuel injection location was assumed equal to the static pressure in the case without combustion, $p_{hole} = 14.88$ bar. The pressure variation for the case without combustion is shown in Figure 18. The mass flow of injected methane per mm vane span and vane for case C1Y was $\dot{w}_{CH_4} = 0.4846 \times 10^{-3}$ kg/s/mm/vane.

Case C1YHF had the same parameters as case C1Y, except for the injection velocity which was $V_{hole} = 270.6$ m/s. Case C5TYHF had the same parameters as C1YHF except for the fuel temperature that was $T_{hole} = 590$ K. Case C1YMA had the same parameters as case C1Y except that the fuel injection velocity was deflected 60 deg toward the pressure side. Case C1YHL had the same parameters as case C1Y except that the injection length was 1.36 mm. The parameters of the five cases presented above are summarized in Table 20.

Parameter	C1Y	C1YHF	C5TYHF	C1YMA	C1YHL
Injection velocity [m/s]	77	270.6	270.6	77	77
Pressure [bar]	14.88	14.88	14.88	14.88	14.88
Temperature [K]	313	313	590	313	313
Injection slot size [mm]	0.55	0.55	0.55	0.55	1.36
Fuel velocity incidence [deg]	0	0	0	60	0

Table 20 – Parameters of Fuel Injection.

The power increase due to *in situ* reheat varied between 0.3% and 4.9 %, as shown in Table 21. The largest power increase corresponded to the largest mass flow rate of fuel, $W_{CH_4} = 13.5 \times 10^{-4}$ kg/s per vane and mm length of vane. The smallest power increase corresponded to the smallest mass flow rate of fuel, $W_{CH_4} = 1.9 \times 10^{-4}$ kg/s per vane and mm length of vane. Note that the correlation between the fuel mass flow rate and the power increase (and implicit temperature increase) is different from the results obtained on the combustion probe.

	C1Y	C1YHF	C5TYHF	C1YMA	C1YHL
Fuel mass flow rate [$\times 10^{-4}$ kg/s/vane/mm]	3.8	13.5	7.2	1.9	9.6
Power increase [%]	0.8	4.9	3.9	0.3	3.1

Table 21 – Power Increase.

The variation of total enthalpy for the three *in situ* reheat cases and for the no combustion case is shown in Figure 19. For clarity, only three combustion cases C1YHF, C5TYHF and C1YHL are shown. The abscissa indicates the axial location. S1 denotes stator 1, R1 denotes rotor 1, etc. The total enthalpy is calculated at inlet and outlet of each row. Depending on the row type, that is, stator or rotor, the total enthalpy is calculated using either the absolute or the relative velocity. The switch between using absolute or relative velocities generates discontinuities between rows. As shown in Figure 19, for all fuel injection cases the total enthalpy increases compared to the no combustion case. The largest enthalpy increase is located on the first rotor, where most of the combustion takes place. The combustion and heat release continue throughout the second stator and rotor, as indicated by the total enthalpy variation shown in Figure 19.

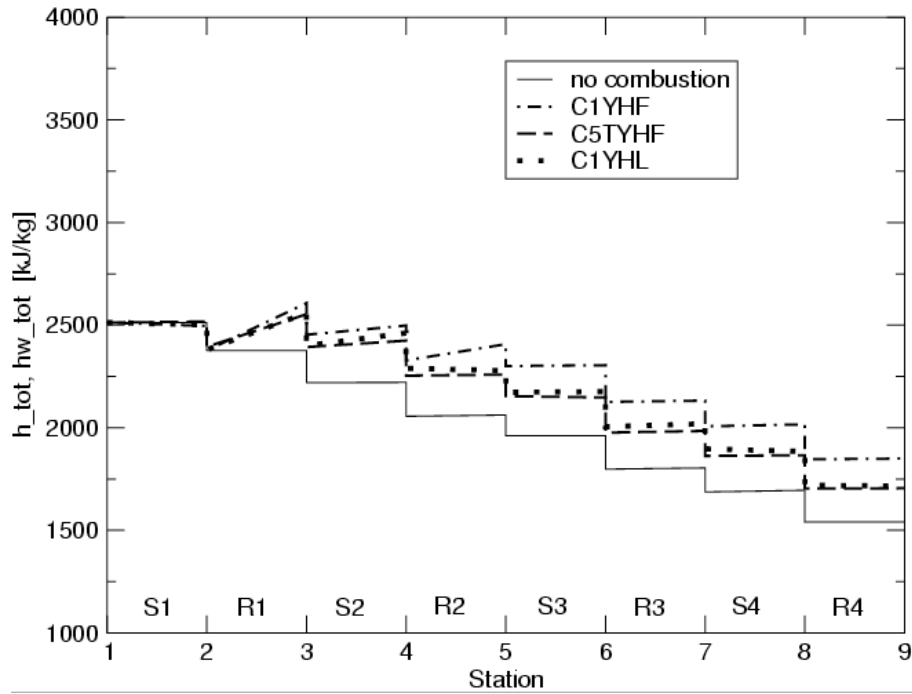


Figure 19 – Variation of averaged total enthalpy (absolute or relative).

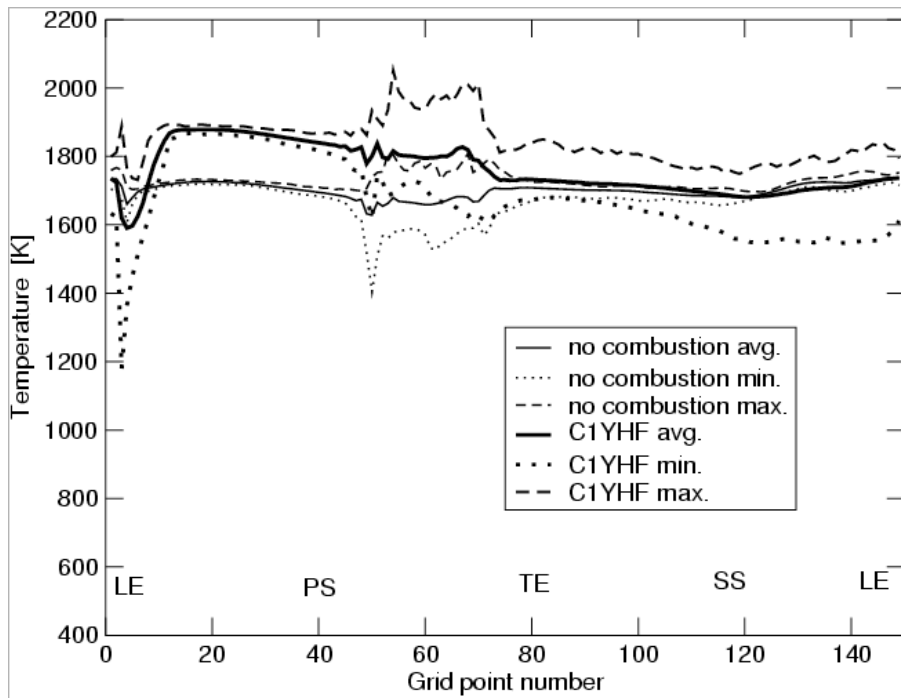


Figure 20 – Variation of stagnation temperature along first row of rotors for case without combustion and case C1YHF of *in situ* reheat.

The stagnation temperature variation along the first row of rotors is strongly influenced by the *in situ* reheat, as shown in Figure 20. Figure 20 shows the averaged, minimum and maximum stagnation temperature for the flow without combustion and for case C1YHF of flow with combustion. On the pressure side, the

averaged temperature of case C1YHF is approximately 180 K larger than the no combustion case temperature. At the leading edge, however, the averaged temperature of case C1YHF is approximately 70 K lower than in the no combustion case. On the suction side, the averaged temperature of case C1YHF is slightly higher than in the no combustion case. On most of the suction side, the averaged temperature of case C1YHF is approximately 15 to 20 K larger than the no combustion case temperature.

The averaged temperature indicates that combustion takes place on the pressure side of the rotor airfoil. The existence of small regions where the averaged temperature of the case with combustion is lower than the average temperature of the case without combustion indicates that combustion is not completed. Consequently, the low enthalpy of the fuel injected reduces locally the airfoil temperature. The maximum temperature in the case with combustion is larger than the maximum temperature in the case without combustion, at any point on the airfoil. On the pressure side, the minimum temperature of the case with combustion is larger than the minimum temperature of the case without combustion. On most of the suction side, however, the minimum temperature of the case with combustion is smaller than the minimum temperature of the case without combustion, indicating that the unburned, cold fuel injected is affecting this region.

The variation of the mass flow rates of species is shown in Figure 21. The mass flow rates of species

$$W_{CH_4} = \rho u Y A = \rho_8 u A \quad (6)$$

was used to assess the variation of the amount of reactants and products. In this assessment done at the postprocessing stage, the diffusion velocity was assumed to be constant and for this reason it was not included in equation (6). For methane, this assumption is less accurate near the injection location where there is a large gradient of the methane mass fraction. Consequently, the mass flow rate of methane in the first stage should be slightly larger compared to the values generated by equation (6).

The variation of the mass flow rate of methane between injection location (more precisely, half a chord downstream of the trailing edge of vane 1) and the exit from the turbine is shown in Table 22 as $\Delta W_{CH_4} / W_{CH_4 \text{ inlet}}$. If the variation of the diffusion velocity would be accounted for, the values of $\Delta W_{CH_4} / W_{CH_4 \text{ inlet}}$ would increase. The reference mass flow rate in Table 22 is $W_{ref} = \rho_{-\infty} V_{ref} (\text{axial chord})^2$, where $V_{ref} = \sqrt{p_{-\infty} / \rho_{-\infty}}$.

These results indicate that approximately 80% of the methane does not burn. Table 22 also shows that the amount of methane injected in case C1YHF is more than double (more precisely 2.25 and 2.33) compared to cases C5TYHF and C1YHL. The highest mass flow rate of burned methane is in case C1YHF, but the highest power increase per mass flow rate of methane injected and the highest power increase per mass flow rate of methane burned are in case C5TYHF.

Case	C1YHF	C5TYHF	C1YHL
W_{CH_4} / W_{CH_4ref}	14.2	6.32	6.08
$\Delta W_{CH_4} / W_{CH_4inlet}[\%]$	15	20.9	21.0
$\Delta W_{CH_4} / W_{CH_4ref}$	2.13	1.32	1.28
$\Delta P / \Delta W_{CH_4}$	2.3	2.95	2.42
$\Delta P / \Delta W_{CH_4}$	0.345	0.617	0.510

Table 22 – Methane variation.

The degree of mixedness is estimated through the mixedness parameter S:

$$S = \frac{1}{\bar{\phi}} \int_{y=0}^{S_{bl}} [\phi(y) - \bar{\phi}]^2 dy \quad (\bar{\phi} \neq 0)$$

with $\bar{\phi}$ being the space averaged value along the region where the integration is performed. It is calculated here for several parameters of interest, such as X_{CH_4} , X_{CO} , T_w^* or T^* , whose distributions are investigated in the cross stream direction between rows, along the y axis. In regions of high non-uniformity values for S are high while in regions of constant ϕ the parameter S becomes zero. As the code used is unsteady, the space dependent quantities (*i.e.*, $\Phi(y)$) were time averaged over a cycle. The values given in Table 23 show the largest values of S for CH_4 , T_w^* and T^* obtained at the exit of the injection row. A similar remark applies for CO .

Case	no combustion	c ly	c lyhf	c5tyhf	c lynna	c lyhl
CO mixedness						
mix_CO_exit_Vane1	0.0	7.33E-03	3.15E-03	5.22E-03	3.68E-03	5.06E-03
mix_CO_exit_Blade1	0.0	6.80E-04	6.27E-04	3.44E-04	8.97E-05	3.76E-04
mix_CO_exit_Vane2	0.0	2.91E-04	1.34E-04	2.40E-04	1.26E-04	1.90E-04
mix_CO_exit_Blade2	0.0	1.12E-04	1.03E-04	4.58E-04	5.65E-05	3.21E-04
mix_CO_exit_Vane3	0.0	2.41E-05	5.12E-05	3.41E-05	2.85E-05	5.82E-05
mix_CO_exit_Blade3	0.0	1.38E-05	1.01E-05	1.36E-04	2.27E-05	8.11E-05
mix_CO_exit_Vane4	0.0	3.62E-05	2.47E-05	3.00E-05	8.06E-06	2.05E-05
mix_CO_exit_Blade4	0.0	7.88E-06	1.50E-05	4.71E-05	1.92E-06	1.40E-05
CH4 mixedness						
mix_CH4_exit_Vane1	0.0	6.24E-01	2.63E+00	1.35E+00	3.05E-01	1.26E+00
mix_CH4_exit_Blade1	0.0	4.12E-02	1.52E-01	7.29E-02	8.87E-03	7.61E-02
mix_CH4_exit_Vane2	0.0	1.73E-02	3.55E-02	1.62E-02	8.97E-03	9.97E-03
mix_CH4_exit_Blade2	0.0	5.63E-03	1.22E-01	2.53E-02	3.80E-03	1.75E-02
mix_CH4_exit_Vane3	0.0	1.58E-03	2.22E-02	1.99E-03	2.46E-03	2.76E-03
mix_CH4_exit_Blade3	0.0	8.33E-04	1.20E-02	6.78E-03	1.88E-03	4.20E-03
mix_CH4_exit_Vane4	0.0	2.17E-03	8.41E-03	1.44E-03	7.50E-04	1.12E-03
mix_CH4_exit_Blade4	0.0	4.78E-04	2.38E-03	2.27E-03	1.50E-04	6.75E-04
T_stagnation mixedness (sse Note)						
mix_Tstag_exit_Vane1	9.61E-05	1.43E-02	3.61E-01	8.36E-02	7.16E-03	9.82E-02
mix_Tstag_exit_Blade1	1.31E-03	2.74E-03	3.37E-02	3.71E-03	1.64E-03	3.89E-03
mix_Tstag_exit_Vane2	3.82E-04	5.50E-04	1.39E-02	2.05E-03	6.24E-04	1.57E-03
mix_Tstag_exit_Blade2	8.27E-04	1.03E-03	3.42E-02	7.09E-03	6.32E-04	5.99E-03
mix_Tstag_exit_Vane3	9.90E-04	1.64E-03	8.54E-03	2.94E-03	5.01E-04	2.19E-03
mix_Tstag_exit_Blade3	1.60E-03	3.89E-03	3.23E-03	5.38E-03	2.64E-03	5.76E-03
mix_Tstag_exit_Vane4	1.84E-03	4.25E-03	5.86E-03	4.78E-03	8.26E-04	3.94E-03
mix_Tstag_exit_Blade4	1.96E-03	3.17E-03	1.01E-03	4.91E-03	3.55E-03	8.92E-04

Table 23 – Mixedness Projection

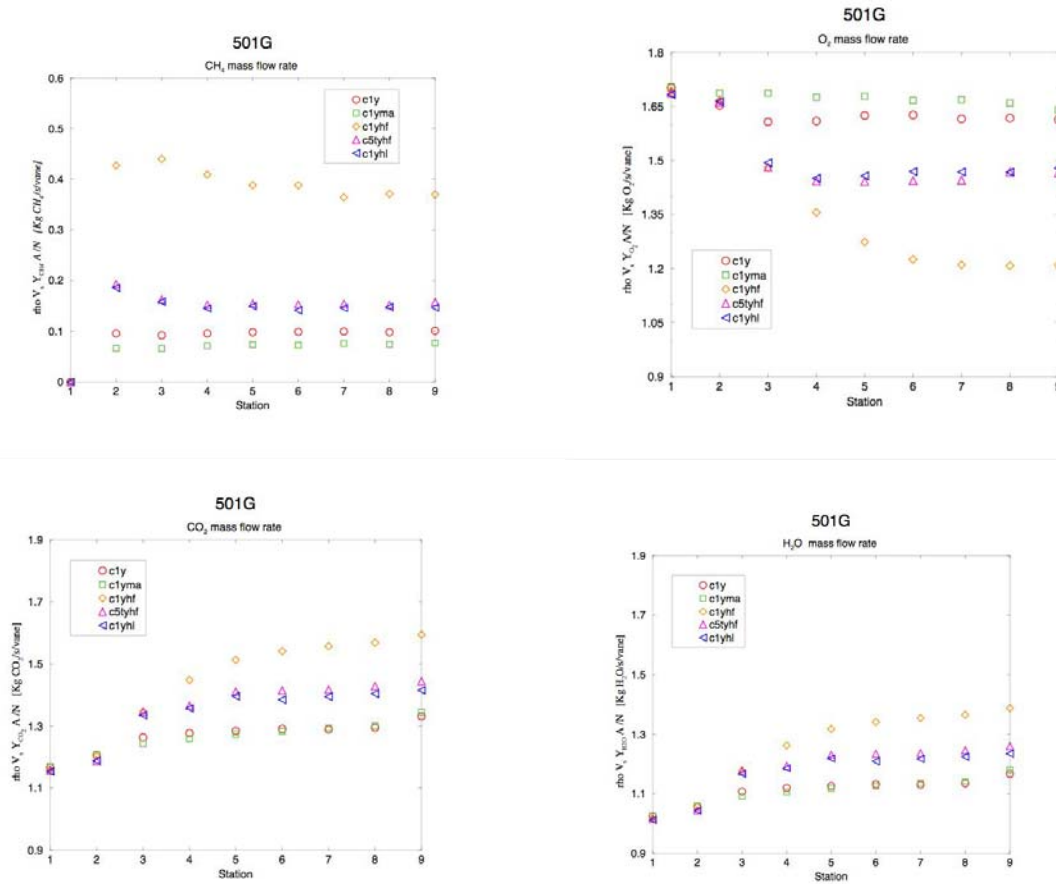


Figure 21 – Variation of CH_4 , O_2 , CO_2 and H_2O mass fractions along the turbine.

4.5 Run Set 2

This section presents and compares the effects of *in situ* reheat in four-stage and five-stage turbines. For each turbine, at least four cases of *in situ* reheat were calculated. The main cases are presented in Table 24.

Cases 1 through 5 cover the four-stage turbine. Cases 6 through 10 cover the five-stage turbine. For the five-stage turbine, only the last four stages are simulated. The first stage in the simulation is the second stage of the five-stage turbine. As a result, what is referred herein as the *i*-th stage of the five-stage turbine is in fact the *i+1*-stage. Cases 1 and 6 represent the no combustion cases for the four-stage and five-stage turbines. In cases 2, 2wide and 7 the fuel injection is done at the trailing edge of vane one. In the cases 2 and 2wide, the mass flow rate of fuel is kept constant while the injection hole diameter and the injection velocity are varied. In cases 3 and 8 the fuel injection is done at the leading edge of the second vane. In cases 4 and 9 the fuel injection is done at the trailing edge of the second vane. In cases 5 and 10 the fuel injection is done at the trailing edge of the third vane.

The effects of *in situ* reheat were investigated by comparing the performances of the turbine-combustor for various cases of fuel injection against the performance of the

same turbine without combustion. Pure methane was injected in all the cases of *in situ* reheat presented herein. The composition of the gas at inlet in the turbine varied slightly for each case.

1	Case	1	2	2wide	3	4	5	6	7	8	9	10
2	Engine	G V1 LE	G V1 TE	G V1 TE	G V2 LE	G V2 TE	G V3 TE	G5 V1 LE	G5 V1 TE	G5 V2 LE	G5 V2 TE	G5 V3 TE
3	Inj. hole location											
4	Injection angle, (rel to vane CL)	N/A	0	0	0	0	0	N/A	0	0	0	0
5	Hole width (mm)	N/A	0.508	0.508	0.508	0.508	0.508	N/A	0.508	0.508	0.508	0.508
6	Main Gas Properties											
7	wt frac O2	0.110	0.116	0.116	0.129	0.133	0.135	0.110	0.116	0.129	0.133	0.135
8	wt frac CO2	0.079	0.074	0.074	0.066	0.063	0.062	0.079	0.074	0.066	0.063	0.062
9	wt frac H2O	0.070	0.067	0.067	0.060	0.058	0.057	0.070	0.067	0.060	0.058	0.057
10	wt frac N2	0.729	0.730	0.730	0.733	0.733	0.734	0.729	0.730	0.733	0.733	0.734
11	wt frac Ar	0.012	0.012	0.012	0.013	0.013	0.013	0.012	0.012	0.013	0.013	0.013
12	Temperature, K	1783	1610	1610	1446	1324	1106	1783	1415	1274	1167	974
13	pressure (bar abs)	18.1	12.9	12.9	9.0	6.4	3	17.8	12.1	8.5	6.0	2.0
14	gas angle (rel to axis), °	0.0	73.0	73.0	-30.0	69.0	64	0.0	73.0	-24.0	69.0	64.0
15	gas velocity (parallel to vane), m/s	122	581	581	257	557	597	122	580	228	522	556
16	Injection Gas Properties											
17	wt frac CH4	N/A	1	1	1	1	1	N/A	1	1	1	1
18	wt frac air	N/A	0	0	0	0	0	N/A	0	0	0	0
19	Temperature @ hole [K]	N/A	700	700	580	580	600	N/A	700	580	580	600
20	(kg injected)/(kg main gas)	0.000	0.005	0.005	0.005	0.005	0.005	0.000	0.010	0.010	0.010	0.010
21												
22	Temperature inlet upstream [K]	1710	1710	1710	1710	1710	1710	1470	1470	1470	1470	1470
23	Stagnation pressure inlet upstream (abs, bar)	17.54	17.54	17.54	17.54	17.54	17.54	16.95	16.95	16.95	16.95	16.95
24	Pressure ratio, p exit static/p inlet total [-]	0.0570	0.0570	0.0570	0.0570	0.0570	0.0570	0.0590	0.0590	0.0590	0.0590	0.0590
25	Pressure @ hole (abs) [bar]	N/A	13.77	13.77	9.82	6.79	3.02	N/A	13.58	8.98	6	2.68
26	Pressure @ hole / p inlet total [-]	N/A	0.7851	0.7851	0.5599	0.3871	0.1722	N/A	0.8012	0.5298	0.3540	0.1581
27	u-velocity/sqrt(pin/rho) @ hole [-]	N/A	0.0745	0.0436	-0.2853	0.1508	0.2838	N/A	0.1832	-0.757	0.4143	0.7745
28	sqrt(pin/rho) @ hole [m/s]	709.86	709.28	709.28	708.97	708.41	708.29	658.16	657.63	657.34	656.82	656.71
29	u-velocity @ hole [m/s]	N/A	52.84	30.92	-202.27	106.83	201.01	N/A	120.48	-497.60	272.12	508.62
30	Inj. Velocity, V [m/s]	N/A	180.73	105.77	-233.56	298.10	458.55	N/A	412.07	-544.70	759.34	1160.25
31	Inj. hole location, I-station	N/A	77	77	1	77	70	N/A	77	1	77	70
32	Inj. hole location, grid number	N/A	2	2	6	6	10	N/A	2	6	6	10
33	Gas constant, R [J/(kg*K)]	294.68	294.2	294.2	293.94	293.48	293.38	294.68	294.2	293.94	293.48	293.38
34	Dynamic viscosity @ hole / Dyn. visc. Inlet [-]	N/A	0.589	0.589	0.521	0.521	0.534	N/A	0.641	0.567	0.567	0.581
35	Dynamic viscosity @ inlet upstream [Pa s]	5.58E-05	5.58E-05	5.58E-05	5.58E-05	5.58E-05	5.58E-05	5.13E-05	5.13E-05	5.13E-05	5.13E-05	5.13E-05
36	Density @ inlet upstream [kg/m3]	3.481	3.487	3.487	3.490	3.495	3.496	3.913	3.919	3.923	3.929	3.930
37	Density @ hole [kg/m3]	N/A	3.796	3.796	3.267	2.259	0.971	N/A	3.743	2.987	1.996	0.862
38	Turbine inlet Mach number [-]	0.152	0.152	0.152	0.152	0.152	0.152	0.164	0.164	0.164	0.164	0.164
39	Velocity at turbine inlet [m/s]	107.90	107.81	107.81	107.76	107.68	107.66	107.94	107.85	107.80	107.72	107.70
40	Reynolds number (turbine inlet)	738636	739238	739238	739565	740145	740271	903498	904235	904634	905343	905497
41	Turbine flow coefficient [-]	0.2792	0.2790	0.2790	0.2789	0.2787	0.2786	0.2793	0.2791	0.2790	0.2788	0.2787
42	Inj. hole diameter use as input [mm]	N/A	0.3	0.508	0.45	0.3	0.3	N/A	0.3	0.45	0.3	0.3
43	Inj. hole effective diameter [mm]	N/A	0.544	0.931	0.489	0.554	0.839	N/A	0.544	0.516	0.554	0.839
44	Main gas mass flow rate [kg/s]	74.67	74.68	74.68	74.67	74.68	74.68	83.94	83.94	83.94	83.94	83.94
45	Fuel inj. mass flow rate [kg/s]	N/A	0.3732	0.3738	0.3731	0.3731	0.3736	N/A	0.8391	0.8395	0.8397	0.8391
46	Fuel inj. / main gas [-]	N/A	0.00500	0.00501	0.00500	0.00500	0.00500	N/A	0.01000	0.01000	0.01000	0.01000
47	Power increase [%]	0	2.6	1.5	0.3	0.2	-0.1	0	0.1	-0.8	-0.8	0
48	Power increase / fuel injection mass flow rate	0	0.03482	0.02009	0.00402	0.00268	-0.00134	0.00000	0.00119	-0.00953	-0.00715	0.00000

Table 24 – Parameter variation for the main cases of *in situ* reheat

4.5.1 Four-Stage Turbine

The largest power increase was obtained by injecting fuel at the trailing edge of the first vane of the four-stage turbine, case 2. The power increase relative to the no combustion case is 2.6%, as shown in Table 24. A smaller power increase (1.5%) was obtained when the injection velocity was reduced from 180 m/s in case 2 to 106 m/s in case 2wide, while keeping the fuel mass flow rate constant. The details of the oxygen variation and velocity vectors near the fuel injection location at the trailing edge of the first vane are shown in Figure 22. The combustion is clustered next to the injection location when the velocity is 106 m/s, while for the larger velocity the combustion extends further away from the vane.

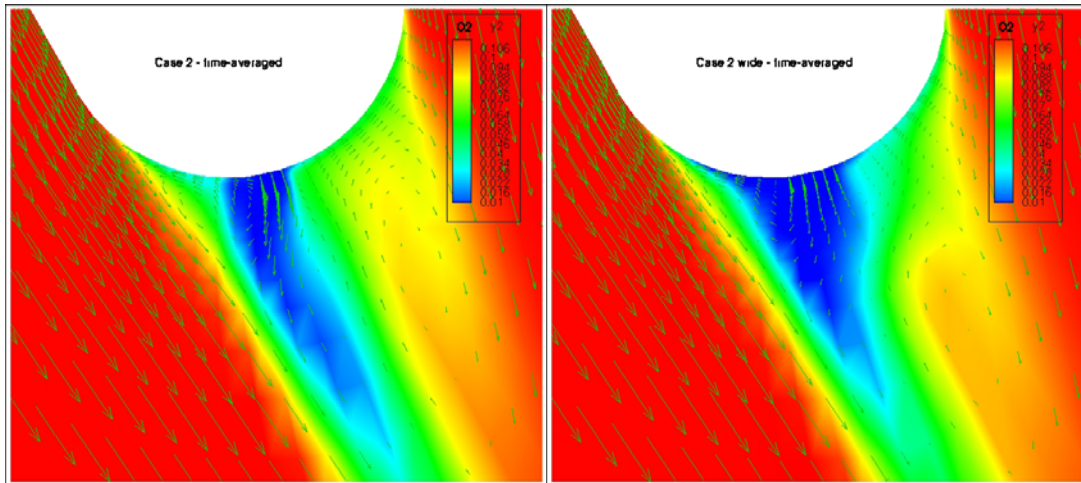


Figure 22 – Oxygen contours and velocity vectors near the injection location for cases 2 and 2wide.

The oxygen contours indicate where combustion takes place, as shown in Figure 23. The combustion is clearly the strongest in case 2 and consequently the power increase is the largest. The oxygen variation is rather small in cases 3 and 5, indicating that combustion is insignificant. A detail of the oxygen contours near the injection location shows that in case 4 the reaction is restricted to a very small region, as shown in Figure 24.

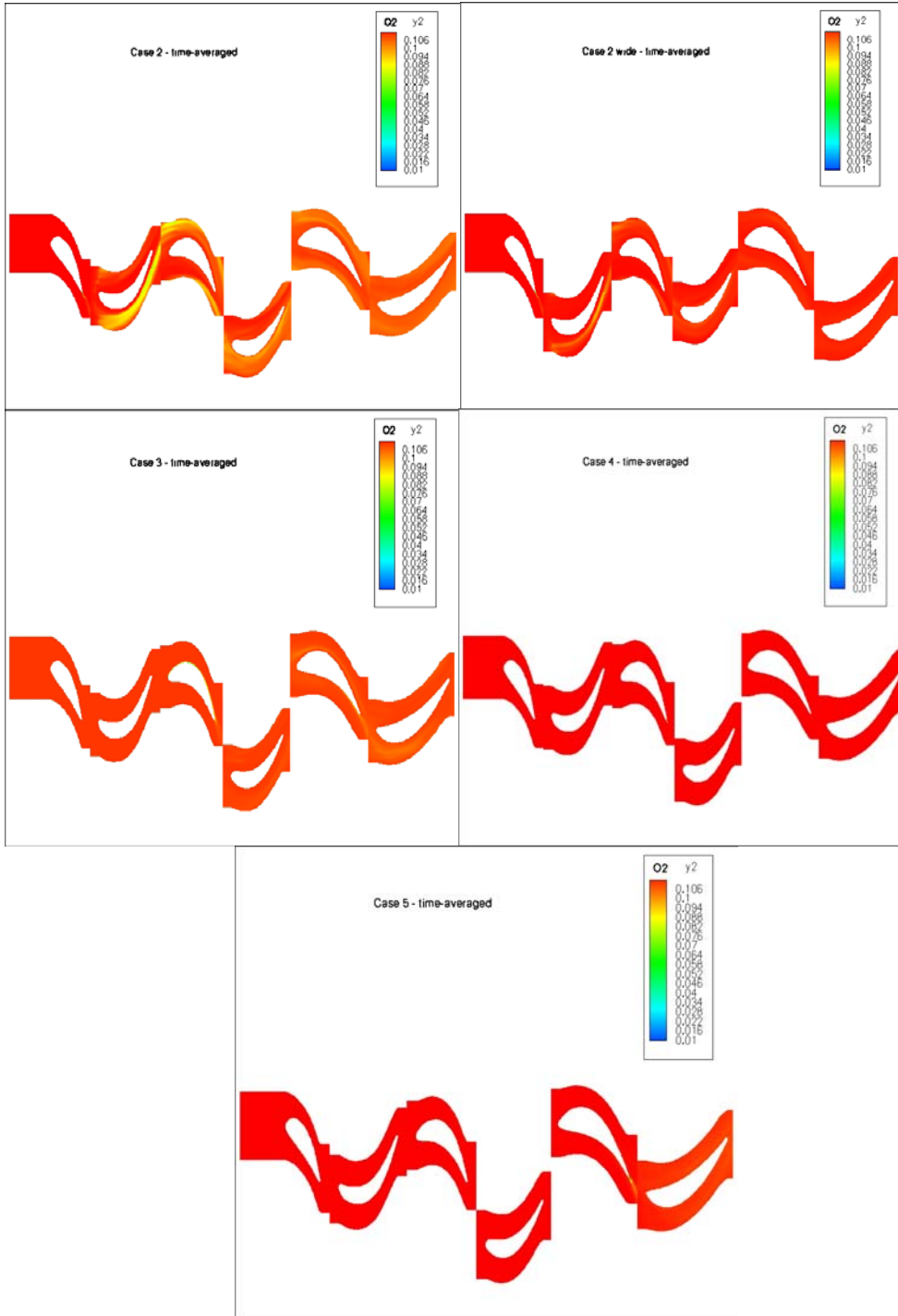


Figure 23 – Oxygen contours for cases 1 through 5.

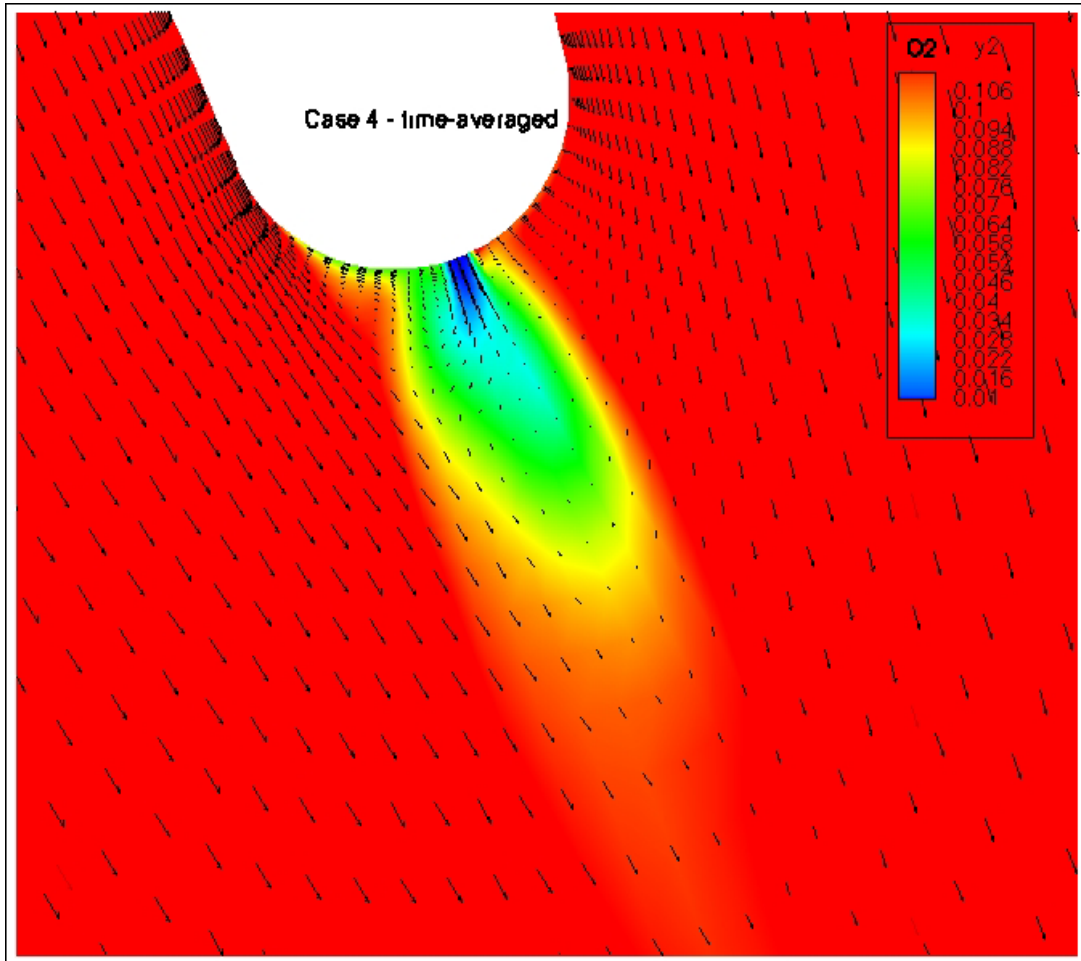


Figure 24 – Oxygen contours and velocity vectors near the injection location for case 4.

The temperature variation for cases 1 through 5 is shown in Figure 25. In cases 2 and 2wide, fuel injection increases the temperature in the first rotor and second stator rows. Temperature does not increase downstream of the injection location in cases 3 through 5 because the fuel does not ignite (or combustion is very localized). Consequently, power increases most in cases 2 and 2wide. Depending on the balance between the entropy increase due to (localized) combustion and the entropy decrease due to the cold fuel injection, the power slightly increases or decreases in cases 3 through 5, as shown in Table 24.

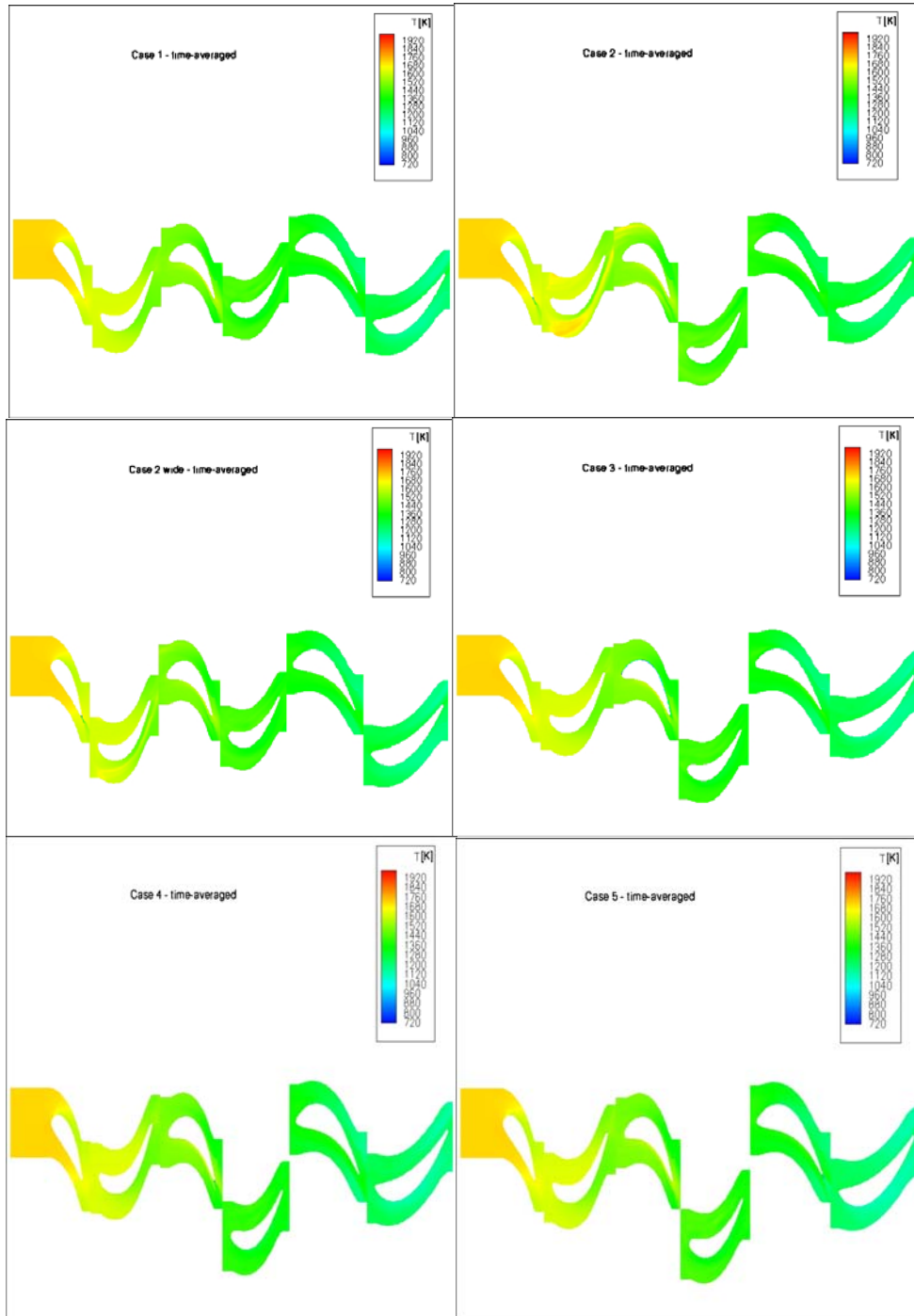


Figure 25 – Temperature contours for cases 1 through 5.

4.5.2 Five-Stage Turbine

Stages 2 through 5 of a five-stage turbine were simulated herein. The mass flow rate of the fuel injected in the turbine was equal to 1% of the mass flow rate of gas entering the turbine. The fuel was injected at the leading edge of the second vane (i.e., the first vane in the numerical simulation – case 6 in Table 24), at the leading edge and trailing edge of the third vane (i.e., second vane in the numerical simulation

– cases 7 and 8), at the trailing edge of the fourth vane (i.e., third vane in the numerical simulation – case 9), and at the trailing edge of the fifth vane (i.e., fourth vane in the numerical simulation – case 10). The power variation shown in Table 24 indicates a smaller power increase compared to the four-stage turbine in spite of the doubled fuel mass flow rate for the five-stage turbine compared to the four-stage turbine.

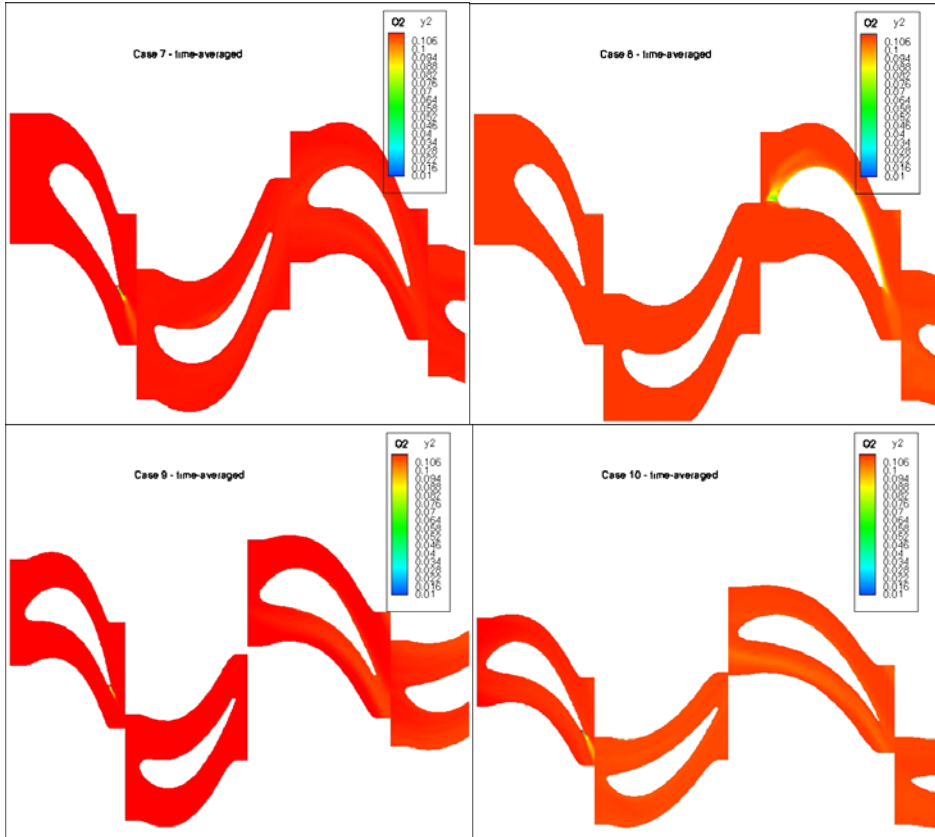


Figure 26 – Oxygen contours for cases 7 through 10.

The variation of the oxygen shown in Figure 26 indicates that combustion is very weak for all the cases of the five-stage turbine. The same conclusion is supported by the temperature contours shown in Figure 27.

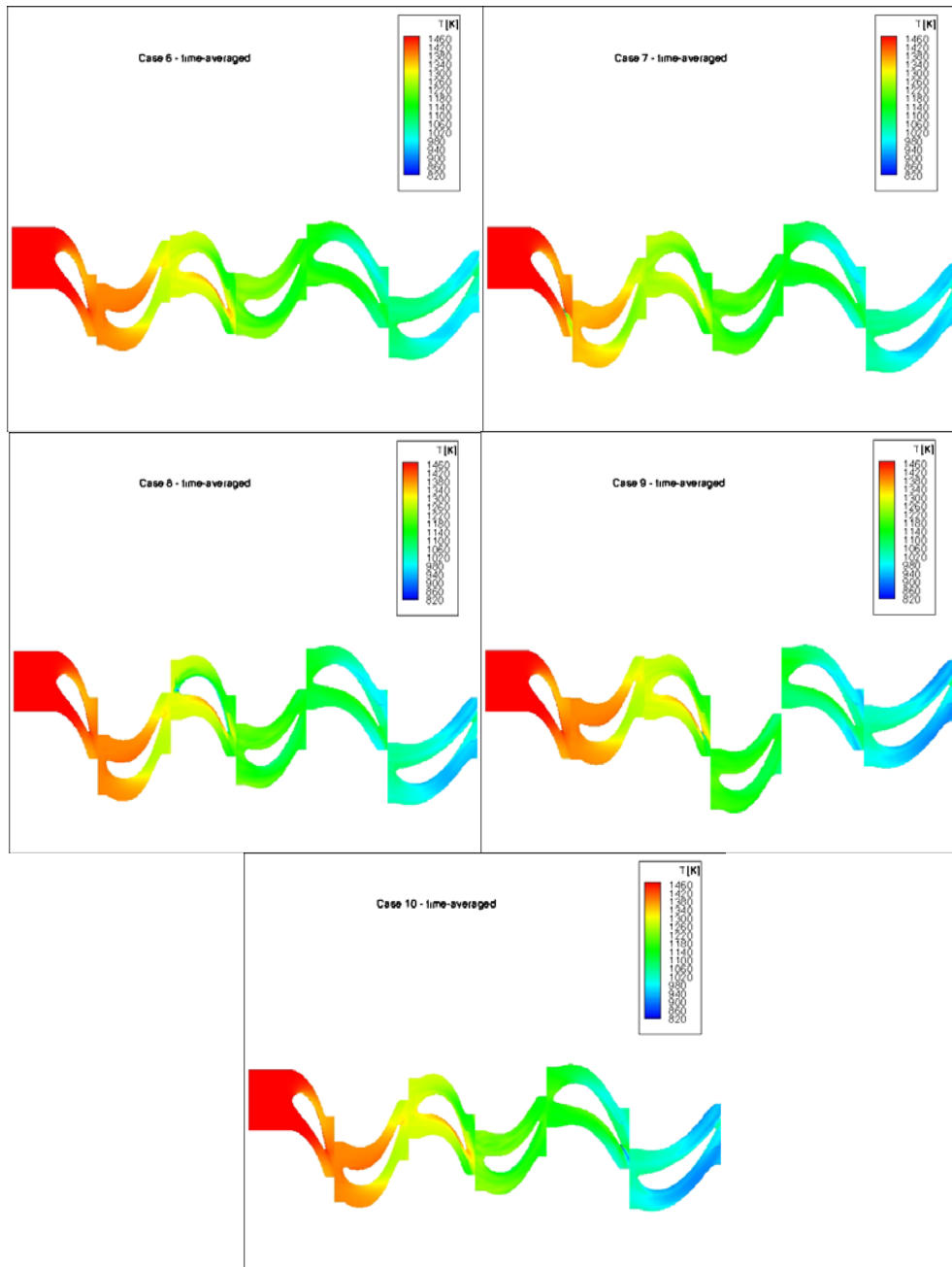


Figure 27 – Temperature contours for cases 6 through 10.

The details of the oxygen variation near the fuel injection situated at leading edge (cases 3 and 8) indicate that the methane flows only on suction side of the vane, as shown in Figure 28. To produce a counter-flow flame, that would have better chances for combustion, the injection location needs to be moved toward the pressure side. A simulation of a new injection location near the leading edge with different injection velocities is necessary in order to determine the parameters needed to anchor the flame.

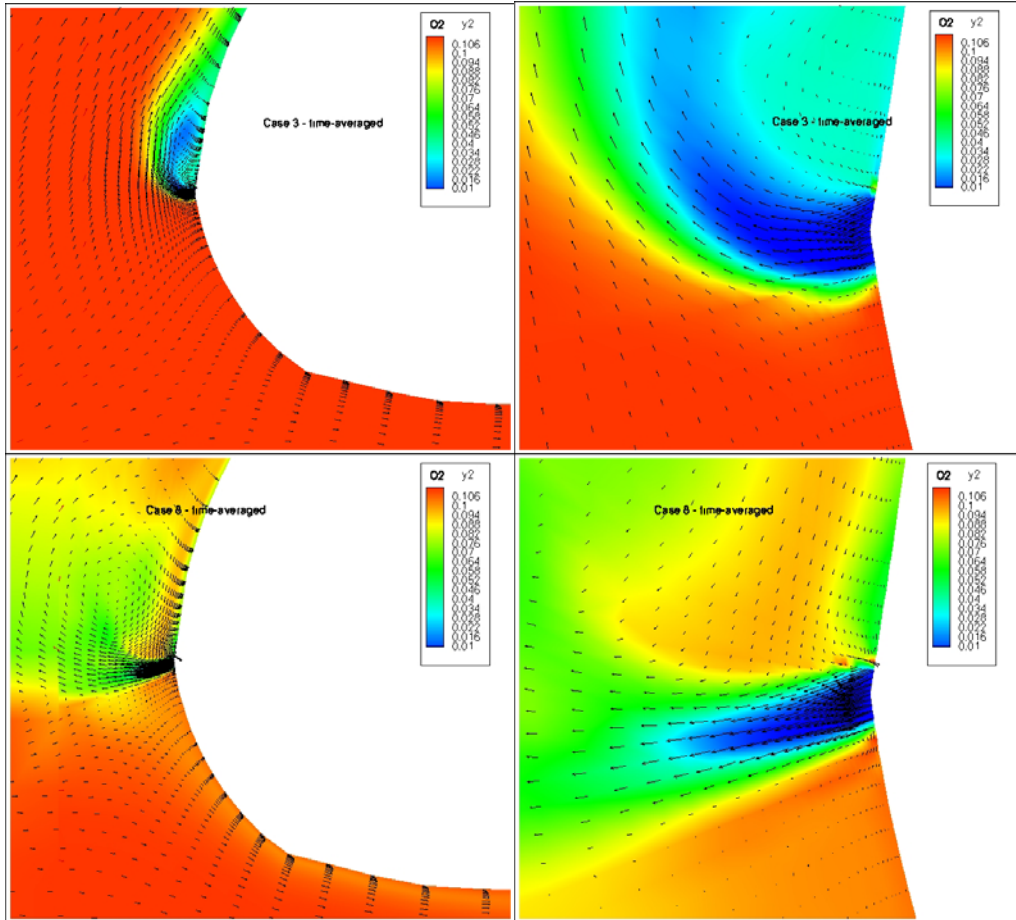


Figure 28 – Oxygen contours and velocity vectors for cases 3 and 8.

4.6 Run Set 3

Ten additional cases were investigated and are presented in this section. These cases, B through K, are similar to the cases 1 through 10 presented above. Case B is similar to case 1, case C is similar to case 2, etc. The differences between cases 1 through 10 and cases B through K consist of small variations of the flow coefficient, fuel injection incidence angle and velocity magnitude. The fuel mass flow rates were similar, except for case K, where the fuel mass flow rate was approximately half the mass flow rate of case 10. The input parameters and the power variation are presented in Table 25.

Similar to the results presented for the cases 1 through 10, the largest power increase was obtained when the fuel was injected at the trailing edge of the first vane, case B. For the other cases, the power increase was significantly smaller. In case I, the fuel did not ignite. As a result, the power variation was negative because of the reduced enthalpy of the fuel.

The difference of the combustion strength between cases C through K is illustrated in Figure 29.

Temperature variation is shown in Figure 30. Clearly the temperature increases most in case C and consequently the power variation is the largest.

1	Case	B	C	D	E	F	G	H	I	J	K
2	Engine	G	G	G	G	G	G5	G5	G5	G5	G5
3	Inj. hole location	V1 LE	V1 TE	V2 LE	V2 TE	V3 TE	V1 LE	V1 TE	V2 LE	V2 TE	V3 TE
4	Injection angle, (rel to vane CL)	N/A	0	0	0	0	N/A	0	0	0	0
5	Main Gas Properties										
6	wt frac O2	0.110	0.116	0.129	0.133	0.1346	0.110	0.116	0.129	0.133	0.135
7	wt frac CO2	0.079	0.074	0.066	0.063	0.0623	0.079	0.074	0.066	0.063	0.062
8	wt frac H2O	0.070	0.067	0.060	0.058	0.057	0.070	0.067	0.060	0.058	0.057
9	wt frac N2	0.729	0.730	0.733	0.733	0.7336	0.729	0.730	0.733	0.733	0.734
10	wt frac Ar	0.012	0.012	0.013	0.013	0.0125	0.012	0.012	0.013	0.013	0.013
11	Injection Gas Properties										
12	wt frac CH4	N/A	1	1	1	1	N/A	1	1	1	1
13	wt frac air	N/A	0	0	0	0	N/A	0	0	0	0
14	Temperature @ hole, K	N/A	700	580	580	600	N/A	700	580	580	600
15											
16	Temperature inlet upstream [K]	1710	1710	1710	1710	1710	1470	1470	1470	1470	1470
17	Stagnation pressure inlet upstream (abs, bar)	17.54	17.54	17.54	17.54	17.54	16.95	16.95	16.95	16.95	16.95
18	Inj. incidence @ hole [deg]	N/A	69.6	0	69.6	60	N/A	69.6	0	69.6	60
19	pressure @ hole (abs, bar)	N/A	13.77	9.82	6.79	3.02	N/A	13.58	8.98	6	2.68
20	u-velocity/sqrt(pinf/rhoinf) @ hole [-]	N/A	0.101	-0.323	0.168	0.369	N/A	0.249	-0.86	0.459	0.46
21	sqrt(pinf/rhoinf) @ hole [m/s]	N/A	717.20	717.20	717.20	717.20	N/A	665.25	665.25	665.25	665.25
22	u-velocity @ hole [m/s]	N/A	72.44	-231.65	120.49	264.65	N/A	165.65	-572.12	305.35	299.36
23	Inj. Velocity, V [m/s]	N/A	207.81	-231.65	345.66	529.29	N/A	475.22	-572.12	876.00	598.73
24	Inj. hole location, l-station	N/A	77	1	77	70	N/A	77	1	77	70
25	Inj. hole location, grid number	N/A	2	6	6	10	N/A	2	6	6	10
26											
27	Dynamic viscosity @ hole / Dyn. visc. Inlet [-]	N/A	0.589	0.521	0.521	0.534	N/A	0.641	0.567	0.567	0.581
28	Dynamic viscosity @ inlet upstream [Pa s]	5.58E-05	5.58E-05	5.58E-05	5.58E-05	5.58E-05	5.13E-05	5.13E-05	5.13E-05	5.13E-05	5.13E-05
29	Density @ inlet upstream [kg/m3]	3.41	3.41	3.41	3.41	3.41	3.83	3.83	3.83	3.83	3.83
30	Density @ hole [kg/m3]	N/A	3.796	3.267	2.259	0.971	N/A	3.743	2.987	1.996	0.862
31	Inj. hole diameter use as input [mm]	N/A	0.3	0.46	0.3	0.3	N/A	0.3	0.46	0.3	0.3
32	Inj. hole effective diameter [mm]	N/A	0.541	0.566	0.554	0.838	N/A	0.541	0.566	0.554	0.838
33	Main gas mass flow rate [kg/s]	74.67	74.68	74.67	74.68	74.68	83.94	83.94	83.94	83.94	83.94
34	Fuel inj. mass flow rate [kg/s]	N/A	0.4268	0.4284	0.4326	0.4307	N/A	0.9623	0.9672	0.9687	0.4325
35	Fuel inj. / main gas [-]	N/A	0.00571	0.00574	0.00579	0.00577	N/A	0.01146	0.01152	0.01154	0.00515
36	Power increase [%]	0	5.5	0.5	0.3	0.2	0	0.6	-0.5	0.4	0.2
37	Power increase / fuel injection mass flow rate	0	0.07365	0.00670	0.00402	0.00268	0.00000	0.00715	-0.00596	0.00477	0.00238

Table 25 – Parameter variation for the additional cases of *in situ* reheat

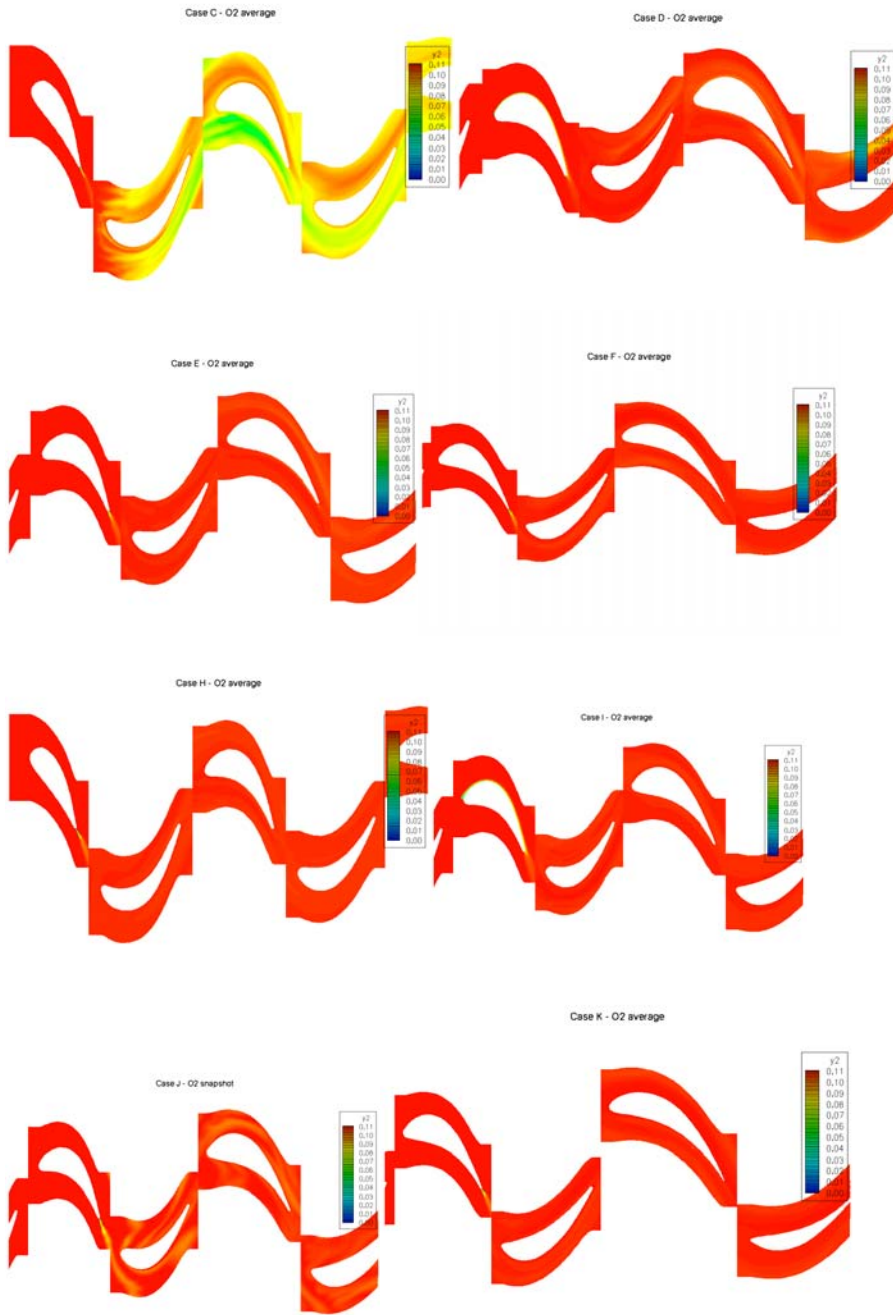


Figure 29 – Oxygen contours for cases C through K.

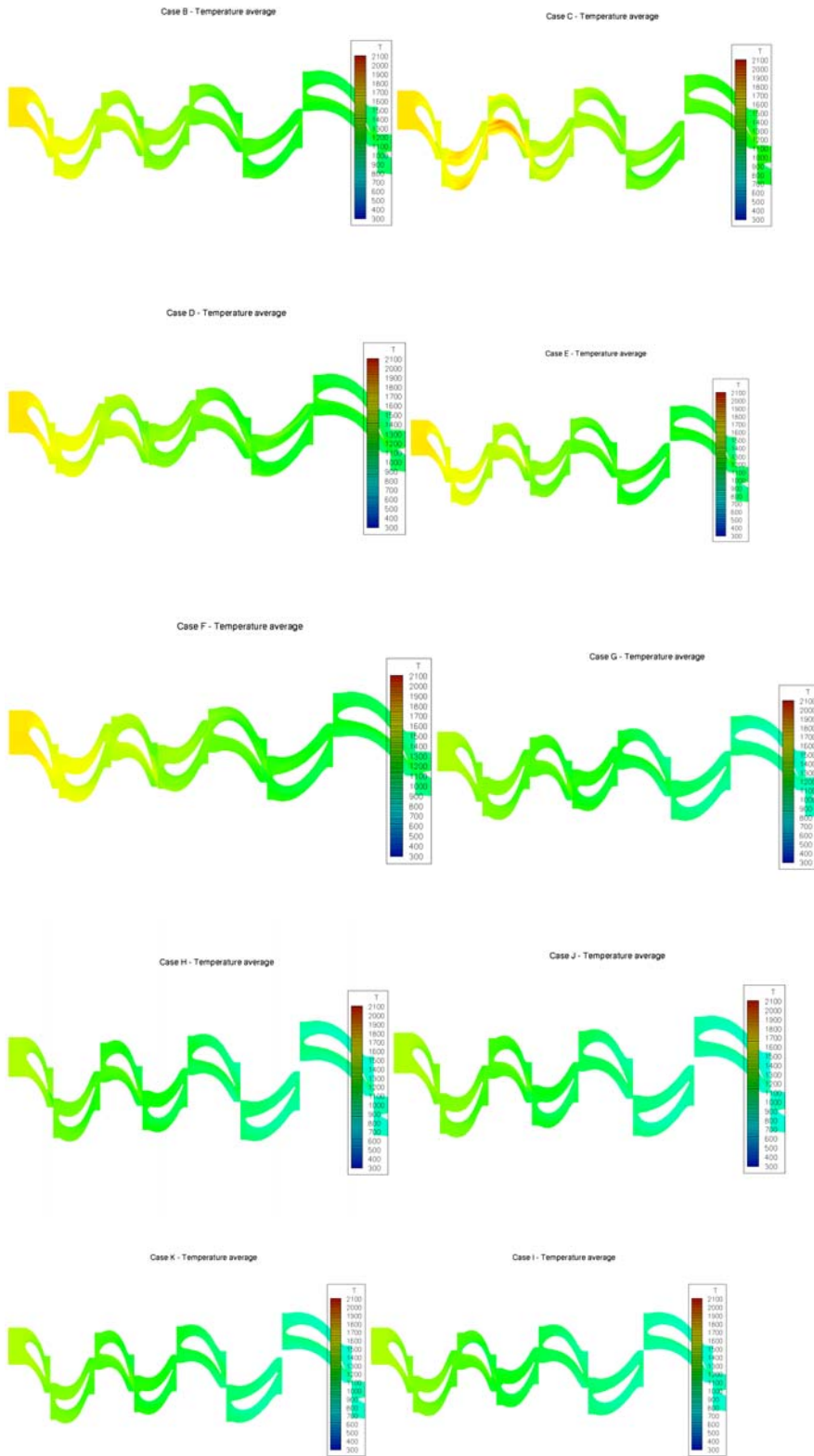


Figure 30 – Temperature contours for cases B through K.

5. CONCLUSIONS

The numerical simulation proved that the combustion model is sufficiently accurate to produce reliable results for parametric studies. The same conclusion results from an on going calibration of the combustion model against detailed experimental data provided by Sandia [4]. The numerical simulation showed that power can be increased by up to 5% with a modest amount of fuel injected in the turbine.

The numerical simulation showed that the best location for fuel injection is at the trailing edge of the inlet guide vane. The flow conditions at the trailing edge promote combustion because (1) the gas velocity in the airfoil's wake is small and (2) the vortices shed at the trailing edge enhance mixing of fuel and oxygen. Consequently, the trailing edge acts as a good flame holder. When the fuel was injected in the second or third stages, however, the combustion either was not initiated or was much weaker compared to the case when the fuel was injected at the inlet guide vane. Reduced temperature and pressure adversely affected *in situ* reheat on second and third vanes.

Fuel injection at the leading edge of second vane did not significantly increase power, although a counter-flow flame has some advantages. The numerical simulation showed that the location of the injection at the leading edge needs to be moved toward the pressure side in order to avoid the flame being swept towards the suction side. The flow unsteadiness at leading edge was another factor that adversely affected the combustion of a fuel injected with constant velocity.

6. RECOMMENDATIONS

The numerical investigation, calibrated by experimental data, showed that combustion in the turbine is possible and that *in situ* reheat increases significantly the power of the turbine. The numerical simulation, however, did not take into account the radial variation effects on *in situ* reheat. Consequently, an important next step in the numerical simulation is the replacement of the quasi-three-dimensional model by a fully three-dimensional model. This will allow to properly capture the radial variation effects on *in situ* reheat. The modeling of the combustion process can be improved as well. One possible improvement is related to the diffusion modeling, where the constant diffusion coefficients will be replaced by binary mixture coefficients. Another improvement will be obtained by replacing the existing two-step combustion model by a five-step combustion model or, even better, by the ARM2 model, a sixteen-step combustion model.

Although the numerical simulation is important, the most important next step is the experimental investigation of a scaled down, one and a half stage turbine-combustor. This experimental investigation will provide critical data on the interaction between the *in situ* reheat, the rotor/stator interaction and the combustor hot streaks. This experiment will also provide the apparatus necessary to investigate different approaches for fuel injection and blade cooling. The experiment can be done at the blow down facility of the Texas A&M University. This facility provides approximately 10 kg/sec at 44 bar for approximately 5 minutes. If necessary, the mass flow rate can be increased by reducing the operating time. A large variety of measurement equipment is also available, including Laser Doppler Anemometry, Particle Image Velocimetry, 18-hole omni-directional probes, etc.

7. REFERENCES

1. Cizmas, P., 1999, Transition and blade count influence on steam turbine clocking, Tech. Rep., Texas Engineering Experiment Station, College Station, Texas.
2. Isvoranu, D. and Cizmas, P, 2003, Numerical simulation of combustion and rotor-stator interaction in a turbine combustor, International Journal of Rotating Machinery, **9** (5), pp. 363-374.
3. Westbrook, C. and Dryer, F., 1981, "Simplified Reaction Mechanisms for the Oxidation of Hydrocarbon Fuels in Flames," Combustion Science and Technology, **27**, pp. 31-43.
4. Barlow, R., Sandia National Laboratories, Private communication.